MECHANICS OF ADVANCED MATERIALS AND STRUCTURES
2020, VOL. 27, NO. 12, 948–964
https://doi.org/10.1080/15376494.2018.1502380

Taylor & Francis
Taylor & Francis Group

ORIGINAL ARTICLE

Exact geometry four-node solid-shell element for stress analysis of functionally graded shell structures via advanced SaS formulation

G. M. Kulikov and S. V. Plotnikova

Laboratory of Intelligent Materials and Structures, Tambov State Technical University, Tambov, Russia

ABSTRACT

The exact geometry four-node solid-shell element formulation using the sampling surfaces (SaS) method is developed. The SaS formulation is based on choosing inside the shell N not equally spaced SaS parallel to the middle surface in order to introduce the displacements of these surfaces as basic shell unknowns. Such choice of unknowns with the use of Lagrange basis polynomials of degree $N-1$ in the through-thickness interpolations of displacements, strains, stresses and material properties leads to a very compact form of the SaS shell formulation. The SaS are located at Chebyshev polynomial nodes that make possible to minimize uniformly the error due to Lagrange interpolation. To implement efficient 3D analytical integration, the extended assumed natural strain method is employed. As a result, the proposed hybrid-mixed solid-shell element exhibits a superior performance in the case of coarse meshes. To circumvent shear and membrane locking, the assumed stress and strain approximations are utilized in the framework of the mixed Hu-Washizu variational formulation. It can be recommended for the 3D stress analysis of thick and thin doubly-curved functionally graded shells because the SaS formulation with only Chebyshev polynomial nodes allows the obtaining of numerical solutions, which asymptotically approach the 3D solutions of elasticity as the number of SaS tends to infinity.

ARTICLE HISTORY
Received 14 July 2018
Accepted 16 July 2018

KEYWORDS
Exact geometry solid-shell element; hybrid-mixed method; sampling surfaces method; 3D stress analysis

1. Introduction

In recent years, a considerable work has been carried out on continuum-based finite elements [1–8] that can handle the analysis of shells satisfactorily. These elements are defined by two layers of nodes at the bottom and top surfaces with three translational degrees of freedom (DOF) per node and known as 6-parameter solid-shell elements. However, the 6-parameter solid-shell formulation based on the complete constitutive equations is deficient because thickness locking occurs. This is due to the fact that the linear displacement field in the thickness direction results in a constant transverse normal strain, which in turn causes artificial stiffening of the shell element in the case of nonvanishing Poisson's ratios. To prevent thickness locking, the 3D constitutive equations have to be modified employing the generalized plane stress conditions [1, 2, 6, 7]. The hybrid stress method [4, 5] in which the transverse normal stress is constant through the shell thickness and the enhanced assumed strain (EAS) method in which the transverse normal strain is enriched in the thickness direction by a linear term [3, 8] are also utilized.

An effective way of using the 3D constitutive equations is to employ the solid-shell element model with seven translational DOF [9–23]. The 7-parameter shell formulation is based on choosing six displacements of the bottom and top surfaces and the transverse displacement of the middle surface as basic shell unknowns. Such formulation is optimal with respect to the number of DOF. To circumvent locking phenomena, the assumed natural strain (ANS) method [9–12, 14, 15], the EAS method [10, 13] and the hybrid-mixed method [13, 18–20] were efficiently applied. The application to functionally graded (FG) shells can be found in contributions [12, 17, 22].

The more general 9-parameter shell formulation is based on introducing nine displacements of external and middle surfaces as shell unknowns [24, 25]. Such choice of unknowns with the consequent use of Lagrange polynomials of the second order in through-thickness approximations of the displacements and strains leads to a robust higher-order shell formulation. Moreover, this model allows the derivation of objective strain-displacement equations, which exactly represent rigid-body motions of the shell in any convected curvilinear coordinate system. Taking into account that the displacement vectors of reference surfaces are resolved in the middle surface basis, the higher-order shell formulation with nine translational DOF is very promising for developing the exact geometry or geometrically exact (GeX) solid-shell elements. The term GeX implies that the parametrization of the middle surface is known a priori and, therefore, the coefficients of the first and second fundamental forms and Christoffel symbols are taken exactly at element nodes.

CONTACT G. M. Kulikov gmkulikov@mail.ru Laboratory of Intelligent Materials and Structures, Tambov State Technical University, Sovetskaya, 106, Tambov 392000, Russia.
Color versions of one or more of the figures in the article can be found online at www.tandfonline.com/umcm.

It should be mentioned that 6- and 7-parameter shell elements without the use of some computational remedies (see e.g., [23]) do not describe properly the transverse stresses in shell structures. To solve the problem, the postprocessing stress recovery technique has to be applied. Nevertheless, to evaluate the through-thickness distribution of transverse stresses in thick and thin shells the higher-order theories must be adopted. The robust GeX shell elements based on the second-, third- and fourth-order theories accounting for thickness stretching for the analysis of laminated and FG structures have been developed in [26–30]. These finite elements exhibit the excellent performance and can be recommended for the 3D stress analysis of shell structures. However, the authors [27] report that the accurate shell elements based on the fourth-order theory do not describe correctly the transverse normal stress especially in the case of thin shells.

The present paper is intended to overcome the aforementioned difficulties and develop the higher-order solid-shell elements that make possible to evaluate all stress components effectively for thick and thin shells. To solve such a problem, the GeX four-node solid-shell element using the SaS concept [31] is proposed. The SaS formulation is based on choosing inside the shell body N SaS $\Omega^1, \Omega^2, ..., \Omega^N$ parallel to the middle surface in order to introduce the displacement vectors $\mathbf{u}^1, \mathbf{u}^2, ..., \mathbf{u}^N$ of these surfaces as basic shell unknowns, where $N \geq 3$. Note that the 9-parameter shell model with three SaS is a particular case of the general SaS formulation. Such choice of unknowns with the use of Lagrange basis polynomials of degree $N-1$ in the through-thickness interpolations of displacements, strains and stresses leads to a very compact form of the SaS shell formulation. Thus, we deal here with the $3N$-parameter shell formulation.

Recently, the SaS formulation has been employed to develop the solid-shell elements for the 3D stress analysis of plates and shells [32–34]. The proposed SaS solid-shell element formulation is characterized by the following features and new developments:

1. We introduce stresses of SaS instead of stress resultants used in previous studies. This novelty allows one to represent the governing equations of the solid-shell element formulation in terms of only SaS variables.
2. Here, the SaS shell formulation [33] is extended to the FG materials. To solve this problem, the material properties are interpolated through the thickness by Lagrange polynomials [34]. Therefore, it does not matter what type of material laws in the thickness direction is utilized. In fact, only the knowledge of the numerical values of material properties on SaS is required.
3. All SaS are located at Chebyshev polynomial nodes, that is, the roots of the Chebyshev polynomial of degree N. Thus, the bottom and top surfaces are not included into a set of SaS. This is important because the SaS formulation with equally spaced SaS [32] does not work properly with the Lagrange polynomials of high degree because of the Runge's phenomenon [35]. This phenomenon can yield the oscillation at the edges of the interval when the user deals with any specific functions similar to the metric functions appearing in strain-displacement equations of the SaS shell formulation (Eq. 6). Therefore, the use of only Chebyshev polynomial nodes inside the shell body can help to improve significantly the behavior of the Lagrange polynomials of high degree because such choice permits one to minimize uniformly the error due to Lagrange interpolation [35]. This means that the numerical solutions through the SaS shell formulation asymptotically approach the 3D solutions of elasticity as the number of SaS tends to infinity.

To prevent element locking, the hybrid-mixed method pioneered by Pian [36] can be applied efficiently. There are three types of hybrid-mixed finite elements in the literature, namely, the hybrid stress elements [4, 5, 13, 37], hybrid strain elements, [1, 2, 13, 19, 38] and hybrid stress-strain elements [6, 7, 18, 20, 24, 25, 39]. These finite elements are based respectively on the Hellinger-Reissner variational principle with displacements and stresses as independent variables, the modified Hellinger-Reissner variational principle in which the displacements and strains are used as primary variables and the Hu-Washizu variational principle depending upon displacements, strains and stresses.

The proposed GeX solid-shell element is based on the hybrid stress-strain method and has computational advantages compared to conventional isoparametric hybrid-mixed finite elements. This is due to the fact that all element matrices require only direct substitutions, that is, no expensive numerical matrix inversion is needed. It is impossible in the framework of isoparametric hybrid-mixed shell element formulations. The important feature of the GeX solid-shell element developed is the use of effective 3D analytical integration by the extended ANS method [24, 40]. This technique makes possible to utilize the coarse meshes and has a great meaning for the numerical modeling of doubly-curved shells with variable curvatures.

2. Three-dimensional description of shell

Consider a shell of the thickness h. Let the middle surface Ω be described by orthogonal curvilinear coordinates θ_1 and θ_2, which are referred to the lines of principal curvatures of its surface. The coordinate θ_3 is oriented along the unit vector $\mathbf{e}_3(\theta_1, \theta_2)$ normal to the middle surface. Introduce the following notations: $\mathbf{e}_\alpha(\theta_1, \theta_2)$ are the orthonormal base vectors of the middle surface; $A_\alpha(\theta_1, \theta_2)$ are the coefficients of the first fundamental form; $k_\alpha(\theta_1, \theta_2)$ are the principal curvatures of the middle surface; $c_\alpha = 1 + k_\alpha\theta_3$ are the components of the shifter tensor; $c^I_\alpha(\theta_1, \theta_2)$ are the components of the shifter tensor at SaS Ω^I depicted in Figure 1:

$$c^I_\alpha = c_\alpha\left(\theta^I_3\right) = 1 + k_\alpha\theta^I_3, \tag{1}$$

where θ^I_3 are the transverse coordinates of SaS defined as

$$\theta^I_3 = -\frac{h}{2}\cos\left(\pi\frac{2I-1}{2N}\right). \tag{2}$$

As can be seen, the SaS are located at Chebyshev polynomial nodes (roots of the Chebyshev polynomial of degree N). Here and in the following developments, the indices I, J, K

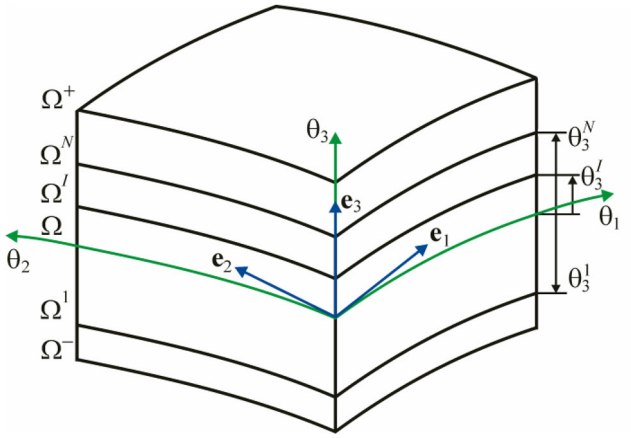

Figure 1. Geometry of the shell.

identify the belonging of any quantity to the SaS and run from 1 to N; Latin indices i, j, k, l range from 1 to 3; Greek indices α, β range from 1 to 2.

In the orthonormal basis $\mathbf{e}_i$, the strain-displacement equations [41] are written as

$$2\varepsilon_{\alpha\beta} = \frac{1}{c_\beta}\lambda_{\alpha\beta} + \frac{1}{c_\alpha}\lambda_{\beta\alpha},$$
$$2\varepsilon_{\alpha 3} = \frac{1}{c_\alpha}\lambda_{3\alpha} + u_{\alpha,3}, \varepsilon_{33} = u_{3,3}, \tag{3}$$

where u_i and ε_{ij} are the displacements and strains; the symbol $(\ldots)_{,i}$ stands for the partial derivatives with respect to coordinates θ_i; $\lambda_{i\alpha}$ are the strain parameters expressed in terms of displacements as follows:

$$\lambda_{\alpha\alpha} = \frac{1}{A_\alpha}u_{\alpha,\alpha} + B_\alpha u_\beta + k_\alpha u_3, \lambda_{\beta\alpha} = \frac{1}{A_\alpha}u_{\beta,\alpha} - B_\alpha u_\alpha,$$
$$\lambda_{3\alpha} = \frac{1}{A_\alpha}u_{3,\alpha} - k_\alpha u_\alpha, B_\alpha = \frac{1}{A_\alpha A_\beta}A_{\alpha,\beta} \quad \text{for} \quad \beta \neq \alpha. \tag{4}$$

The main idea of the SaS formulation [31] is to introduce the displacements of SaS $u_i^I(\theta_1, \theta_2)$ as basic shell unknowns:

$$u_i^I = u_i\left(\theta_3^I\right). \tag{5}$$

The strains of SaS $\varepsilon_{ij}^I(\theta_1, \theta_2)$ can be also introduced for convenience

$$2\varepsilon_{\alpha\beta}^I = 2\varepsilon_{\alpha\beta}\left(\theta_3^I\right) = \frac{1}{c_\beta^I}\lambda_{\alpha\beta}^I + \frac{1}{c_\alpha^I}\lambda_{\beta\alpha}^I,$$
$$2\varepsilon_{\alpha 3}^I = 2\varepsilon_{\alpha 3}\left(\theta_3^I\right) = \beta_\alpha^I + \frac{1}{c_\alpha^I}\lambda_{3\alpha}^I, \varepsilon_{33}^I = \varepsilon_{33}\left(\theta_3^I\right) = \beta_3^I, \tag{6}$$
$$\beta_i^I = u_{i,3}\left(\theta_3^I\right),$$

where $\beta_i^I(\theta_1, \theta_2)$ are the values of the derivative of displacements with respect to thickness coordinate on SaS; $\lambda_{i\alpha}^I(\theta_1, \theta_2)$ are the strain parameters of SaS given by

$$\lambda_{\alpha\alpha}^I = \lambda_{\alpha\alpha}\left(\theta_3^I\right) = \frac{1}{A_\alpha}u_{\alpha,\alpha}^I + B_\alpha u_\beta^I + k_\alpha u_3^I,$$
$$\lambda_{\beta\alpha}^I = \lambda_{\beta\alpha}\left(\theta_3^I\right) = \frac{1}{A_\alpha}u_{\beta,\alpha}^I - B_\alpha u_\alpha^I,$$
$$\lambda_{3\alpha}^I = \lambda_{3\alpha}\left(\theta_3^I\right) = \frac{1}{A_\alpha}u_{3,\alpha}^I - k_\alpha u_\alpha^I, B_\alpha = \frac{1}{A_\alpha A_\beta}A_{\alpha,\beta} \text{ for } \beta \neq \alpha. \tag{7}$$

3. Displacement and strain distributions in thickness direction

We start now with the first fundamental assumption of the proposed higher-order shell theory. Let us assume that the displacements are distributed through the thickness as follows:

$$u_i = \sum_I L^I u_i^I, \tag{8}$$

where $L^I(\theta_3)$ are the Lagrange basis polynomials of degree $N-1$ defined as

$$L^I = \prod_{J \neq I}\frac{\theta_3 - \theta_3^J}{\theta_3^I - \theta_3^J}. \tag{9}$$

The use of Eqs. (6) and (8) yields

$$\beta_i^I = \sum_J M^J\left(\theta_3^I\right)u_i^J, \tag{10}$$

where $M^I = L^I_{,3}$ are the polynomials of degree $N-2$; their values on SaS are

$$M^J\left(\theta_3^I\right) = \frac{1}{\theta_3^J - \theta_3^I}\prod_{K \neq I,J}\frac{\theta_3^I - \theta_3^K}{\theta_3^J - \theta_3^K} \quad \text{for} \quad J \neq I,$$
$$M^I\left(\theta_3^I\right) = -\sum_{J \neq I} M^J\left(\theta_3^I\right). \tag{11}$$

It is seen that the key functions β_i^I of the proposed higher-order shell formulation are represented according to Eq. (10) as a linear combination of displacements of SaS u_i^J.

Proposition 1. The functions $\beta_i^1, \beta_i^2, \ldots, \beta_i^N$ are linearly dependent, that is, there exist numbers $\alpha_1, \alpha_2, \ldots, \alpha_N$, which are not all zero, such that

$$\sum_I \alpha_I \beta_i^I = 0. \tag{12}$$

The proof of this statement can be found in [33].

The following step consists in a choice of the consistent approximation of strains through the thickness of the shell. It is apparent that the strain distribution should be chosen similar to displacement distribution (Eq. 8), that is,

$$\varepsilon_{ij} = \sum_I L^I \varepsilon_{ij}^I. \tag{13}$$

Proposition 2. Strain-displacement equations (6, 7, 10), and (13) exactly represent rigid-body motions of a shell in any convected curvilinear coordinate system.

The proof of this statement is presented in [42].

4. Hu-Washizu variational equation

To develop the hybrid stress-strain solid-shell element formulation, we invoke the Hu-Washizu variational principle in which displacements, strains and stresses are utilized as independent variables:

$$\delta J_{\mathrm{HW}} = 0, \tag{14}$$

$$J_{\mathrm{HW}}=\iint_{\Omega}\int_{-h/2}^{h/2}\left[\frac{1}{2}e_{ij}C_{ijkl}e_{kl}-\sigma_{ij}(e_{ij}-\varepsilon_{ij})\right]A_1A_2c_1c_2d\theta_1d\theta_2d\theta_3-W, \tag{15}$$

$$W=\iint_{\Omega}(c_1^+c_2^+p_i^+u_i^+-c_1^-c_2^-p_i^-u_i^-)A_1A_2d\theta_1d\theta_2+W_{\Sigma}, \tag{16}$$

where σ_{ij} are the stresses; e_{ij} are the displacement-independent strains; C_{ijkl} are the elastic constants of the material; u_i^- and u_i^+ are the displacements of bottom and top surfaces Ω^- and Ω^+; c_α^- and c_α^+ are the components of the shifter tensor on outer surfaces; p_i^- and p_i^+ are the tractions acting on outer surfaces; W_Σ is the work done by external loads applied to the edge surface Σ. As usual, the summation on repeated Latin indices is implied.

According to the SaS technique, we introduce the last three assumptions for stresses, displacement-independent strains, and material properties choosing their through-thickness distributions similar to distributions (8) and (13):

$$\sigma_{ij}=\sum_I L^I\sigma_{ij}^I, \tag{17}$$

$$e_{ij}=\sum_I L^I e_{ij}^I, \tag{18}$$

$$C_{ijkl}=\sum_I L^I C_{ijkl}^I, \tag{19}$$

where $\sigma_{ij}^I=\sigma_{ij}(\theta_3^I)$ are the stresses of SaS; $e_{ij}^I=e_{ij}(\theta_3^I)$ are the displacement-independent strains of SaS; $C_{ijkl}^I=C_{ijkl}(\theta_3^I)$ are the material properties of SaS.

Substituting through the thickness distributions (13, 17–19) in (15) and introducing the weighted coefficients

$$\Lambda^{IJK}=\int_{-h/2}^{h/2}L^IL^JL^Kc_1c_2d\theta_3,\ \Gamma^{IJ}=\int_{-h/2}^{h/2}L^IL^Jc_1c_2d\theta_3, \tag{20}$$

we can write the Hu-Washizu functional in terms of SaS variables

$$J_{\mathrm{HW}}=\int\int_{\Omega}\sum_I\sum_J\left[\sum_K\frac{1}{2}\Lambda^{IJK}(\mathbf{e}^I)^{\mathrm{T}}\mathbf{C}^J\mathbf{e}^K-\Gamma^{IJ}(\boldsymbol{\sigma}^I)^{\mathrm{T}}(\mathbf{e}^J-\boldsymbol{\varepsilon}^J)\right]A_1A_2d\theta_1d\theta_2-W, \tag{21}$$

where

$$\boldsymbol{\varepsilon}^I=\left[\varepsilon_{11}^I\ \varepsilon_{22}^I\ \varepsilon_{33}^I\ 2\varepsilon_{12}^I\ 2\varepsilon_{13}^I\ 2\varepsilon_{23}^I\right]^{\mathrm{T}},\quad \mathbf{e}^I=\left[e_{11}^I\ e_{22}^I\ e_{33}^I\ 2e_{12}^I\ 2e_{13}^I\ 2e_{23}^I\right]^{\mathrm{T}},$$

$$\boldsymbol{\sigma}^I=\left[\sigma_{11}^I\ \sigma_{22}^I\ \sigma_{33}^I\ \sigma_{12}^I\ \sigma_{13}^I\ \sigma_{23}^I\right]^{\mathrm{T}}, \tag{22}$$

$$\mathbf{C}^J=\begin{bmatrix}C_{1111}^J & C_{1122}^J & C_{1133}^J & C_{1112}^J & 0 & 0\\ C_{2211}^J & C_{2222}^J & C_{2233}^J & C_{2212}^J & 0 & 0\\ C_{3311}^J & C_{3322}^J & C_{3333}^J & C_{3312}^J & 0 & 0\\ C_{1211}^J & C_{1222}^J & C_{1233}^J & C_{1212}^J & 0 & 0\\ 0 & 0 & 0 & 0 & C_{1313}^J & C_{1323}^J\\ 0 & 0 & 0 & 0 & C_{2313}^J & C_{2323}^J\end{bmatrix}.$$

5. ANS four-node solid-shell element

The finite element formulation is based on the simple interpolation of the shell via GeX four-node solid-shell elements

$$u_i^I=\sum_r N_r u_{ir}^I, \tag{23}$$

$$N_r=\frac{1}{4}(1+n_{1r}\xi_1)(1+n_{2r}\xi_2), \tag{24}$$

$$n_{1r}=\begin{cases}1 \text{ for } r=1,4\\ -1 \text{ for } r=2,3\end{cases},\quad n_{2r}=\begin{cases}1 \text{ for } r=1,2\\ -1 \text{ for } r=3,4\end{cases},$$

where $N_r(\xi_1,\xi_2)$ are the bilinear shape functions of the element; u_{ir}^I are the displacements of SaS at element nodes; $\xi_\alpha=(\theta_\alpha-d_\alpha)/\ell_\alpha$ are the normalized curvilinear coordinates (Figure 2); $2\ell_\alpha$ are the lengths of the element in (θ_1,θ_2)-space; the nodal index r runs from 1 to 4.

To implement the efficient analytical integration throughout the finite element, the extended ANS method [40] is utilized to interpolate the displacement-dependent strains

$$\boldsymbol{\varepsilon}^I=\sum_r N_r\boldsymbol{\varepsilon}_r^I,\quad \boldsymbol{\varepsilon}_r^I=\left[\varepsilon_{11r}^I\ \varepsilon_{22r}^I\ \varepsilon_{33r}^I\ 2\varepsilon_{12r}^I\ 2\varepsilon_{13r}^I\ 2\varepsilon_{23r}^I\right]^{\mathrm{T}}, \tag{25}$$

where ε_{ijr}^I are the strains of SaS at element nodes.

The main idea of such approach can be traced back to the ANS method developed by many scientists (see e.g. [43–45]) to cure the isoparametric finite elements from shear and membrane locking. In contrast to the conventional formulation, we treat the term ANS in a broader sense. In the GeX four-node solid-shell element formulation, the displacement-dependent strains of SaS are assumed to vary bilinearly throughout the biunit square in (ξ_1,ξ_2)-space. The extended ANS method (25) makes it possible to utilize the element nodes as sampling points that helps to avoid the use of Gauss numerical integration.

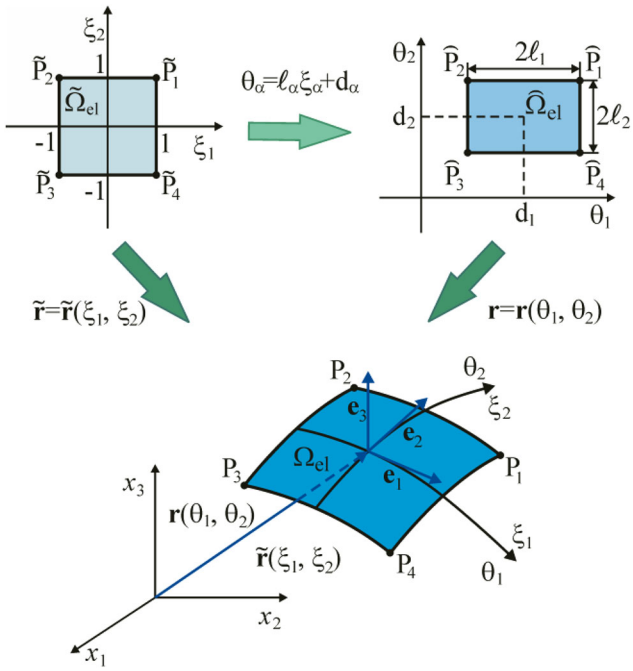

Figure 2. Biunit square in (ξ_1,ξ_2)-space mapped into the middle surface of the GeX solid-shell element in (x_1,x_2,x_3)-space.

Remark 1. In order to circumvent curvature thickness locking for the isoparametric four-node solid-shell element, Betsch and Stein [46] proposed to utilize the bilinear interpolation (25) for the transverse normal strain. It is apparent that curvature thickness locking is not related to the GeX four-node solid-shell element because it can handle the arbitrary geometry of surfaces properly. We advocate the use of the extended ANS method (25) for all components of the strain tensor to implement the effective analytical integration throughout the element.

The strains of SaS at element nodes can be expressed as

$$\boldsymbol{\varepsilon}_r^I = \mathbf{B}_r^I \mathbf{q}, \tag{26}$$

where $\mathbf{B}_r^I$ are the *constant* strain-displacement matrices of order $6 \times 12N$ presented in Appendix A; $\mathbf{q}$ is the element displacement vector given by

$$\mathbf{q} = \left[\mathbf{q}_1^{\mathrm{T}} \mathbf{q}_2^{\mathrm{T}} \mathbf{q}_3^{\mathrm{T}} \mathbf{q}_4^{\mathrm{T}}\right]^{\mathrm{T}}, \quad \mathbf{q}_r = \left[u_{1r}^1 u_{2r}^1 u_{3r}^1 u_{1r}^2 u_{2r}^2 u_{3r}^2 \ldots u_{1r}^N u_{2r}^N u_{3r}^N\right]^{\mathrm{T}}. \tag{27}$$

For further developments it is convenient to rewrite the ANS interpolation (25) in the following form:

$$\boldsymbol{\varepsilon}^I = \sum_{r_1, r_2} (\xi_1)^{r_1} (\xi_2)^{r_2} \boldsymbol{\varepsilon}_{r_1 r_2}^I, \tag{28}$$

$$\boldsymbol{\varepsilon}_{r_1 r_2}^I = \mathbf{B}_{r_1 r_2}^I \mathbf{q}, \tag{29}$$

where

$$\begin{aligned}
&\boldsymbol{\varepsilon}_{r_1 r_2}^I = \left[\varepsilon_{11 r_1 r_2}^I \varepsilon_{22 r_1 r_2}^I \varepsilon_{33 r_1 r_2}^I 2\varepsilon_{12 r_1 r_2}^I 2\varepsilon_{13 r_1 r_2}^I 2\varepsilon_{23 r_1 r_2}^I\right]^{\mathrm{T}}, \\
&\mathbf{B}_{00}^I = \frac{1}{4}\left(\mathbf{B}_1^I + \mathbf{B}_2^I + \mathbf{B}_3^I + \mathbf{B}_4^I\right), \mathbf{B}_{01}^I = \frac{1}{4}\left(\mathbf{B}_1^I + \mathbf{B}_2^I - \mathbf{B}_3^I - \mathbf{B}_4^I\right), \\
&\mathbf{B}_{10}^I = \frac{1}{4}\left(\mathbf{B}_1^I - \mathbf{B}_2^I - \mathbf{B}_3^I + \mathbf{B}_4^I\right), \mathbf{B}_{11}^I = \frac{1}{4}\left(\mathbf{B}_1^I - \mathbf{B}_2^I + \mathbf{B}_3^I - \mathbf{B}_4^I\right).
\end{aligned} \tag{30}$$

Here and below, the indices r_1 and r_2 run from 0 to 1.

6. Hybrid stress-strain solid-shell element formulation

To circumvent shear and membrane locking and obtain no spurious zero energy modes, the robust stress interpolation [24] is utilized

$$\boldsymbol{\sigma}^I = \sum_{r_1 + r_2 < 2} (\xi_1)^{r_1} (\xi_2)^{r_2} \mathbf{Q}_{r_1 r_2} \boldsymbol{\sigma}_{r_1 r_2}^I, \tag{31}$$

$$\begin{aligned}
&\boldsymbol{\sigma}_{00}^I = \left[\varphi_1^I \varphi_2^I \varphi_3^I \varphi_4^I \varphi_5^I \varphi_6^I\right]^{\mathrm{T}}, \quad \boldsymbol{\sigma}_{01}^I = \left[\varphi_7^I \varphi_9^I \varphi_{11}^I\right]^{\mathrm{T}}, \\
&\boldsymbol{\sigma}_{10}^I = \left[\varphi_8^I \varphi_{10}^I \varphi_{12}^I\right]^{\mathrm{T}},
\end{aligned}$$

where $\mathbf{Q}_{r_1 r_2}$ are the projective matrices defined as

$$\begin{aligned}
\mathbf{Q}_{00} &= \begin{bmatrix} 1 & 0 & 0 & 0 & 0 & 0 \\ 0 & 1 & 0 & 0 & 0 & 0 \\ 0 & 0 & 1 & 0 & 0 & 0 \\ 0 & 0 & 0 & 1 & 0 & 0 \\ 0 & 0 & 0 & 0 & 1 & 0 \\ 0 & 0 & 0 & 0 & 0 & 1 \end{bmatrix}, \mathbf{Q}_{01} = \begin{bmatrix} 1 & 0 & 0 \\ 0 & 0 & 0 \\ 0 & 1 & 0 \\ 0 & 0 & 0 \\ 0 & 0 & 1 \\ 0 & 0 & 0 \end{bmatrix}, \\
\mathbf{Q}_{10} &= \begin{bmatrix} 0 & 0 & 0 \\ 1 & 0 & 0 \\ 0 & 1 & 0 \\ 0 & 0 & 0 \\ 0 & 0 & 0 \\ 0 & 0 & 1 \end{bmatrix}.
\end{aligned} \tag{32}$$

The similar interpolation can be used for displacement-independent strains, that is,

$$\mathbf{e}^I = \sum_{r_1 + r_2 < 2} (\xi_1)^{r_1} (\xi_2)^{r_2} \mathbf{Q}_{r_1 r_2} \mathbf{e}_{r_1 r_2}^I, \tag{33}$$

$$\begin{aligned}
&\mathbf{e}_{00}^I = \left[\psi_1^I \ \psi_2^I \ \psi_3^I \ \psi_4^I \ \psi_5^I \ \psi_6^I\right]^{\mathrm{T}}, \quad \mathbf{e}_{01}^I = \left[\psi_7^I \ \psi_9^I \ \psi_{11}^I\right]^{\mathrm{T}}, \\
&\mathbf{e}_{10}^I = \left[\psi_8^I \ \psi_{10}^I \ \psi_{12}^I\right]^{\mathrm{T}}.
\end{aligned}$$

Substituting interpolations (23, 28, 31), and (33) into the Hu-Washizu variational principle (14) and (21) and replacing the metric product $A_1 A_2$ in surface integrals by its value at the element center, one can integrate analytically throughout the finite element. As a result, the following equilibrium equations of the GeX hybrid-mixed solid-shell element are obtained:

$$\sum_J \Gamma^{IJ} \left(\mathbf{e}_{r_1 r_2}^J - \mathbf{Q}_{r_1 r_2}^{\mathrm{T}} \mathbf{B}_{r_1 r_2}^J \mathbf{q}\right) = 0 \quad \text{for} \quad r_1 + r_2 < 2, \tag{34}$$

$$\sum_J \left(\Gamma^{IJ} \boldsymbol{\sigma}_{r_1 r_2}^J - \sum_K \Lambda^{IJK} \mathbf{Q}_{r_1 r_2}^{\mathrm{T}} \mathbf{C}^J \mathbf{Q}_{r_1 r_2} \mathbf{e}_{r_1 r_2}^K\right) = 0 \quad \text{for} \quad r_1 + r_2 < 2, \tag{35}$$

$$\sum_I \sum_J \Gamma^{IJ} \sum_{r_1 + r_2 < 2} \frac{1}{3^{r_1 + r_2}} \left(\mathbf{B}_{r_1 r_2}^I\right)^{\mathrm{T}} \mathbf{Q}_{r_1 r_2} \boldsymbol{\sigma}_{r_1 r_2}^J = \mathbf{F}, \tag{36}$$

where $\mathbf{F}$ is the surface traction vector.

Owing to Proposition B1 in Appendix B, Eq. (34) can be simplified

$$\mathbf{e}_{r_1 r_2}^I - \mathbf{Q}_{r_1 r_2}^{\mathrm{T}} \mathbf{B}_{r_1 r_2}^I \mathbf{q} = 0 \quad \text{for} \quad r_1 + r_2 < 2. \tag{37}$$

Because of interpolations (31) and (33) the stresses and displacement-independent strains are discontinuous at the element boundaries. Hence the vectors $\boldsymbol{\sigma}_{r_1 r_2}^I$ and $\mathbf{e}_{r_1 r_2}^I$ can be eliminated from Eqs. (35–37) that leads to finite element equations

$$\mathbf{K}\mathbf{q} = \mathbf{F}, \tag{38}$$

where $\mathbf{K}$ is the element stiffness matrix of order $12N \times 12N$ given by

$$\mathbf{K} = \sum_I \sum_J \sum_K \Lambda^{IJK} \sum_{r_1 + r_2 < 2} \frac{1}{3^{r_1 + r_2}} \left(\mathbf{B}_{r_1 r_2}^I\right)^{\mathrm{T}} \mathbf{Q}_{r_1 r_2} \mathbf{Q}_{r_1 r_2}^{\mathrm{T}} \mathbf{C}^J \mathbf{Q}_{r_1 r_2} \mathbf{Q}_{r_1 r_2}^{\mathrm{T}} \mathbf{B}_{r_1 r_2}^K. \tag{39}$$

It is worth noting that the element stiffness matrix (39) is evaluated without expensive numerical matrix inversion that is impossible with conventional isoparametric hybrid-mixed solid-shell elements. Furthermore, the stiffness matrix is calculated by using analytical integration throughout the element. Thus, the GeX hybrid stress-strain solid-shell element developed is economical and efficient because it additionally permits the use of coarse meshes as demonstrated in benchmarks considered in Section 8.

7. Assessment of rank of element stiffness matrix

The stress and displacement-independent strain interpolations have to be selected such that the four-node solid-shell element would be free of shear and membrane locking and

they must be as simple as possible. Due to the strain interpolation (33), we introduce 12 assumed strain parameters $\psi_1^I, \psi_2^I, ..., \psi_{12}^I$ for each SaS, that is, $12N$ for all SaS. It seems to be excessive for the SaS solid-shell element with $12N$ displacement DOF. However, there exist *six* dependent strain modes exactly, which provide a correct rank of the element stiffness matrix. This statement has been proved analytically [47] for the SaS hybrid-mixed quadrilateral plate element.

Concerning the GeX four-node solid-shell element it is still possible to describe three dependent strain modes because there is a link between displacement-dependent and displacement-independent strains of SaS

$$\mathbf{e}^I_{r_1r_2} = \mathbf{Q}^{\mathrm{T}}_{r_1r_2}\boldsymbol{\varepsilon}^I_{r_1r_2} \quad \text{for} \quad r_1 + r_2 < 2, \tag{40}$$

which follows directly from Eqs. (29) and (37). Using notations (30, 32), and (33), one obtains

$$\psi_3^I = \varepsilon^I_{3300}, \quad \psi_9^I = \varepsilon^I_{3301}, \quad \psi_{10}^I = \varepsilon^I_{3310}. \tag{41}$$

According to Proposition 1 and strain-displacement equations (6) there exist numbers $\alpha_1, \alpha_2, ..., \alpha_N$ such that

$$\sum_I \alpha_I \varepsilon^I_{33} = 0. \tag{42}$$

The use of Eqs. (28), (41), and (42) yields the first three dependent strain modes

$$\sum_I \alpha_I \psi_3^I = 0, \quad \sum_I \alpha_I \psi_9^I = 0, \quad \sum_I \alpha_I \psi_{10}^I = 0. \tag{43}$$

The other three dependent strain modes cannot be obtained analytically; only numeric calculations make possible to evaluate the eigenvalue problem. Therefore, we consider a few shell elements frequently used in applications: square plate, cylindrical shell, spherical shell and hyperbolic shell elements made of nonhomogeneous material with $\nu = 0.3$ and

$$E = E^- \mathrm{e}^{\alpha(\theta_3 + h/2)}, \quad -h/2 \le \theta_3 \le h/2, \tag{44}$$

where $E^- = 10^9$ is the Young modulus on the bottom surface; α is the material gradient index. The results of calculating eigenvalues with three and five SaS are shown in Figures 3–6. It is seen that six zero eigenvalues are clearly observed for homogeneous and nonhomogeneous shells but the results for the hyperbolic shell are better using more SaS.

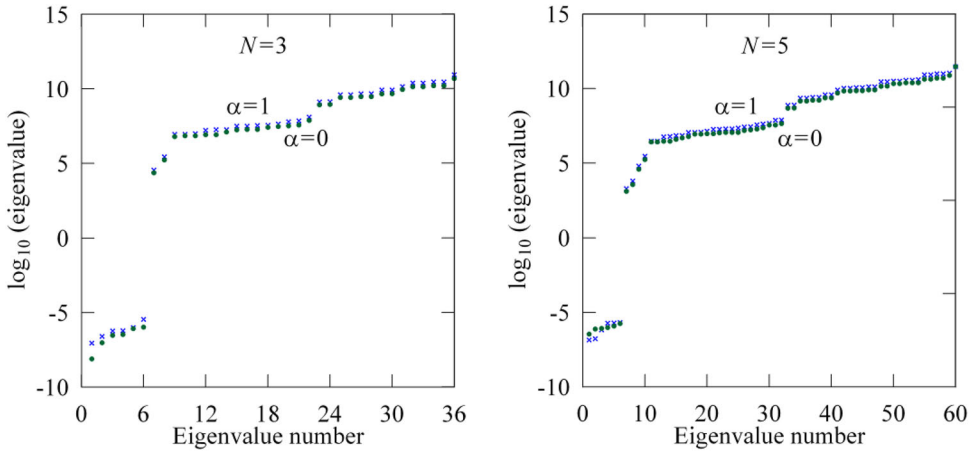

Figure 3. Eigenvalues of the square plate element with $a = 1$ and $h = 0.1$.

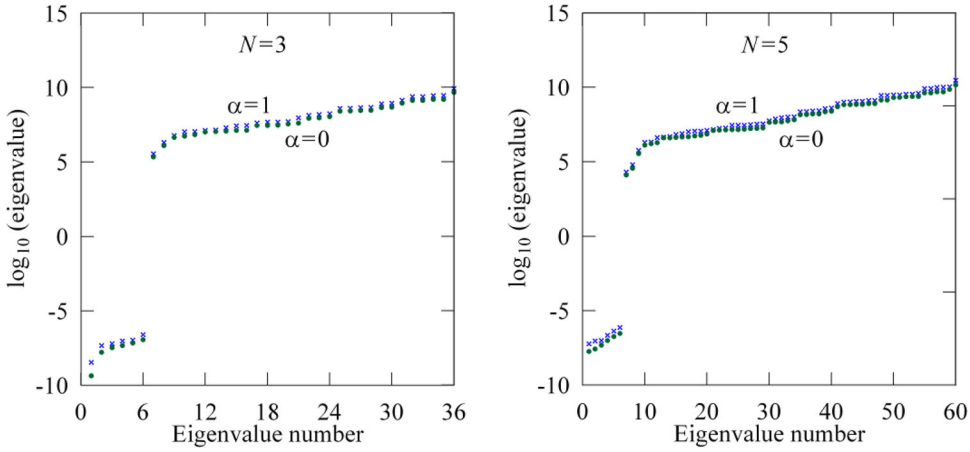

Figure 4. Eigenvalues of the cylindrical shell element ($L/4 \le \theta_1 \le L/2, \pi/8 \le \theta_2 \le \pi/4$) depicted in Figure 10 with $L = R = 1$ and $h = 0.1$.

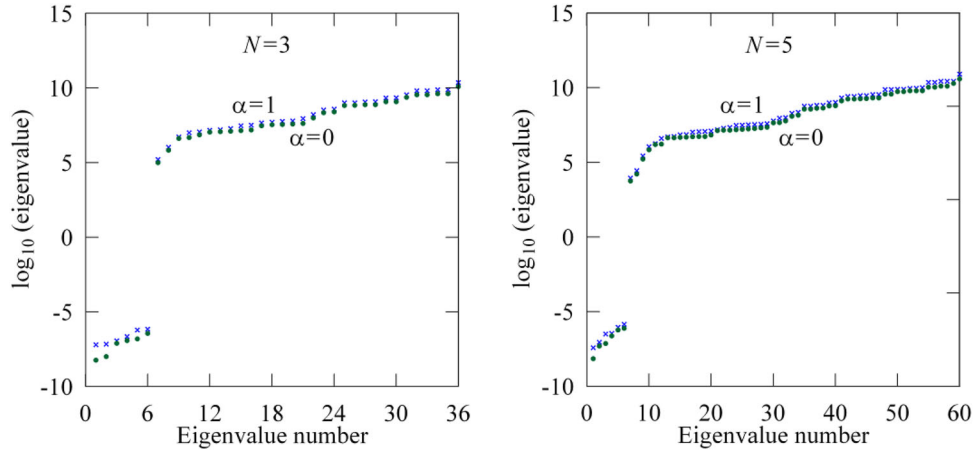

Figure 5. Eigenvalues of the spherical shell element ($\pi/4 \le \theta_1 \le 3\pi/8, 0 \le \theta_2 \le \pi/4$) depicted in Figure 12 with $R = 1$, $\theta_0 = 0$ and $h = 0.1$.

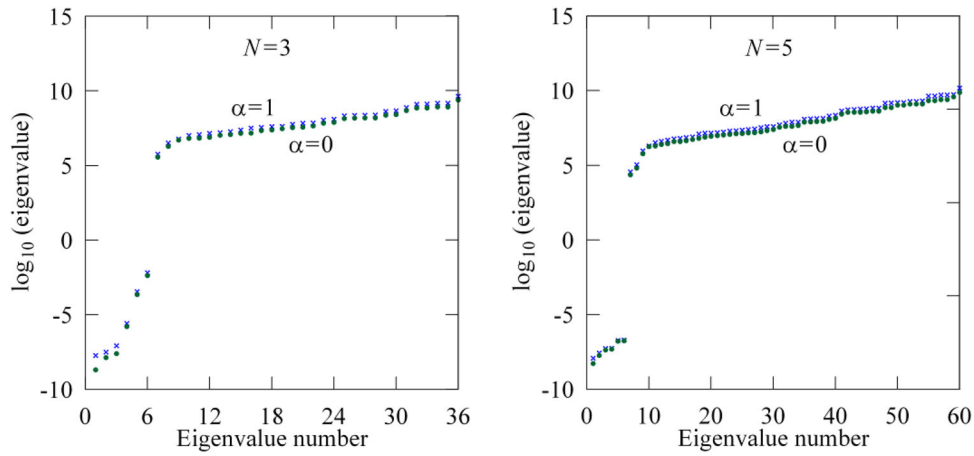

Figure 6. Eigenvalues of the hyperbolic shell element ($L/4 \le \theta_1 \le L/2, \pi/8 \le \theta_2 \le \pi/4$) depicted in Figure 15 with $L = R = 1$, $r = 0.5$ and $h = 0.1$.

8. Numerical examples

The performance of the GeX hybrid-mixed four-node solid-shell element denoted by the GeXSaS4 element is evaluated with 3D exact solutions of elasticity considered in Sections 8.1 and 8.3. The pinched cylindrical shell with rigid diaphragms and the pinched FG hyperbolic shell are also considered as benchmarks.

8.1. Simply supported composite cylindrical shell under sinusoidal loading

First, we study a simply supported cylindrical shell with dimensions of $L/R = 4$ subjected to sinusoidal loading distributed on the bottom surface

$$p_3^- = -p_0 \sin\frac{\pi\theta_1}{L}\cos 4\theta_2,$$

where L and R are the length and radius of a shell; θ_1 and θ_2 are the axial and circumferential coordinates of the middle surface. The shell is made of the unidirectional composite with the fibers oriented in the circumferential direction. The mechanical properties are taken to be $E_L = 25E_T$, $G_{LT} = 0.5E_T$, $G_{TT} = 0.2E_T$, $E_T = 10^6$, $\nu_{LT} = \nu_{TT} = 0.25$, where subscripts L and T refer to the fiber and transverse directions of the composite.

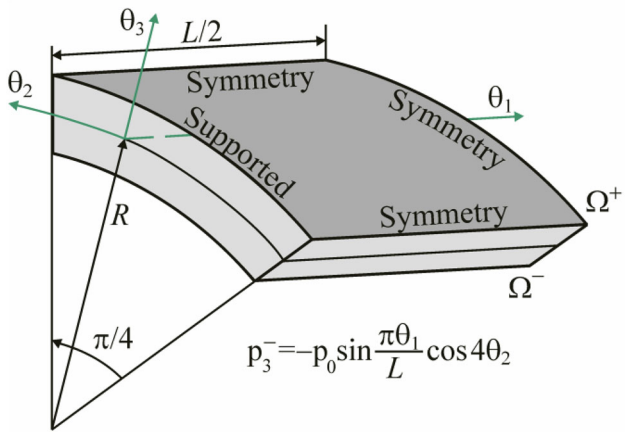

Figure 7. One sixteenth of the simply supported composite cylindrical shell under sinusoidal loading modeled by regular $4n \times 4n$ meshes with $n = 1$, 2, 4, 8, 12 and 16.

Owing to symmetry of the problem, only one sixteenth of the shell depicted in Figure 7 is discretized by regular meshes of GeXSaS4 elements. To compare the derived

results with the exact solution of elasticity [48], we introduce the following dimensionless variables at crucial points as functions of the dimensionless thickness coordinate:

$$\begin{aligned}
\bar{u}_1(z) &= 10E_{\mathrm{L}}\ h^2 u_1(0,0,z)/R^3 p_0,\\
\bar{u}_2(z) &= 10E_{\mathrm{L}}\ h^2 u_2(L/2,\pi/8,z)/R^3 p_0,\\
\bar{u}_3(z) &= 10E_{\mathrm{L}}\ h^3 u_3(L/2,0,z)/R^4 p_0,\\
\bar{\sigma}_{11}(z) &= 100h^2\sigma_{11}(L/2,0,z)/R^2 p_0,\\
\bar{\sigma}_{22}(z) &= 10h^2\sigma_{22}(L/2,0,z)/R^2 p_0,\\
\bar{\sigma}_{12}(z) &= 100h^2\sigma_{12}(0,\pi/8,z)/R^2 p_0,\\
\bar{\sigma}_{13}(z) &= 100h\sigma_{13}(0,0,z)/R p_0,\\
\bar{\sigma}_{23}(z) &= 10h\sigma_{23}(L/2,\pi/8,z)/R p_0,\\
\bar{\sigma}_{33}(z) &= \sigma_{33}(L/2,0,z)/p_0, z=\theta_3/h,
\end{aligned} \tag{45}$$

where $p_0 = 1$ and $R = 1$.

Table 1 lists the results of the convergence study due to increasing the number of SaS for a moderately thick cylindrical shell using the 64×64 mesh. A comparison with the Varadan–Bhaskar exact solution [48] is also presented. It is seen that the GeXSaS4 element provides three or four right digits for displacements and stresses since seven SaS located at Chebyshev polynomial nodes. Figure 8 shows the distributions of dimensionless variables (45) through the thickness of the shell for different values of the slenderness ratio R/h using nine SaS and the same mesh. These results demonstrate convincingly the high potential of the GeXSaS4 element because the boundary conditions on bottom and top surfaces for transverse stresses are satisfied correctly. Figure 9 displays the results of the convergence study due to mesh refinement through normalized displacements and stresses for different slenderness ratios choosing nine SaS and regular $4n \times 4n$ meshes. The reference values are provided by authors' exact SaS solution [31]. As can be seen, the GeXSaS4 element behaves well in the case of coarse meshes even for the transverse normal stress.

8.2. Pinched cylindrical shell with rigid diaphragms

To illustrate the capability of the GeXSaS4 element to overcome shear and membrane locking phenomena (shear locking is much greater than membrane locking [49]) and to compare it with high performance isoparametric four-node shell elements [50–52], we study one of the most demanding tests. Consider a short cylindrical shell supported by two rigid diaphragms at the ends and loaded by two opposite concentrated loads at its middle section.

Due to symmetry of the problem, only one octant of the shell is modeled by regular meshes of GeXSaS4 elements depicted in Figure 10. The shell parameters are taken to be $R = 300$, $L = 300$, $E = 3 \times 10^6$, $\nu = 0.3$ and $F = 1$. Table 2 shows the transverse displacement at the point A and the comparison with [50–52] is also given. The analytical answer of the classic shell theory is -1.8248×10^{-5} [52]. The use of five SaS and a fine mesh 128×128 yields -1.845×10^{-5}. A slightly less value of -1.844×10^{-5} is obtained by using the eight-node brick element Solid45 [53] with four elements in the thickness direction that corresponds to the choice of five SaS. It is seen that the GeXSaS4 shell element is the best performer, whereas the other elements are too stiff in the case of coarse meshes.

For the further analysis it is convenient to introduce the dimensionless variables at any point $\mathrm{P}(\theta_1, \theta_2)$ belonging to the middle surface as follows:

$$\begin{aligned}
\bar{u}_1(\mathrm{P},z) &= 100Eh^2 u_1(\mathrm{P},z)/RF,\\
\bar{u}_3(\mathrm{P},z) &= Eh^2 u_3(\mathrm{P},z)/RF,\\
\bar{\sigma}_{11}(\mathrm{P},z) &= 100h^2\sigma_{11}(\mathrm{P},z)/F,\\
\bar{\sigma}_{22}(\mathrm{P},z) &= 100h^2\sigma_{22}(\mathrm{P},z)/F,\\
\bar{\sigma}_{12}(\mathrm{P},z) &= 100h^2\sigma_{12}(\mathrm{P},z)/F,\\
\bar{\sigma}_{13}(\mathrm{P},z) &= 100Rh\sigma_{13}(\mathrm{P},z)/F,\\
\bar{\sigma}_{23}(\mathrm{P},z) &= 100Rh\sigma_{23}(\mathrm{P},z)/F,\\
\bar{\sigma}_{33}(\mathrm{P},z) &= 100Rh\sigma_{33}(\mathrm{P},z)/F, z=\theta_3/h.
\end{aligned} \tag{46}$$

Table 3 lists the results of the convergence study due to increasing the number of SaS by means of dimensionless variables (46) at points B and C using the 64×64 mesh. Figure 11 displays the through-thickness distributions of stresses for different slenderness ratios R/h choosing seven SaS inside the shell. The results are compared with the Solid45 element [53] using the same fine mesh and six elements in the thickness direction that corresponds to a chosen number of SaS. One can see that the Solid45 element leads to a poor prediction for the transverse stresses. It should be noted that it is impossible to satisfy the boundary conditions on bottom and top surfaces by choosing 12 and even 16 elements in the thickness direction.

8.3. Pressurized nonhomogeneous spherical shell

Next, we consider a nonhomogeneous spherical shell subjected to uniform pressure p_0 acting on the inner surface. Owing to symmetry, one sixteenth of the shell is discretized by regular $4n \times 1$ meshes shown in Figure 12. The coefficients of the first and second fundamental forms and Christoffel symbols of the spherical surface with a hole at the top are given by

$$\begin{aligned}
&A_1 = R, \quad A_2 = R\sin\theta_1, \quad k_1 = 1/R, \quad k_2 = 1/R, B_1 = 0,\\
&B_2 = \frac{\cos\theta_1}{R\sin\theta_1}, \quad \theta_1 \in [\theta_0, \pi/2].
\end{aligned} \tag{47}$$

Table 1. Convergence study for a composite cylindrical shell with $R/h = 10$ using 64×64 mesh.

	$\bar{u}_1(0.5)$	$\bar{u}_2(-0.5)$	$\bar{u}_3(0)$	$\bar{\sigma}_{11}(0.5)$	$\bar{\sigma}_{22}(0.5)$	$\bar{\sigma}_{12}(-0.5)$	$\bar{\sigma}_{13}(0)$	$\bar{\sigma}_{23}(0)$	$\bar{\sigma}_{33}(0)$
$N = 3$	−0.7668	−3.098	0.8536	0.4571	3.584	−0.3696	0.3369	−2.523	−1.091
$N = 5$	−0.8213	−3.392	0.9186	0.6521	4.046	−0.4118	0.5217	−3.714	−1.388
$N = 7$	−0.8215	−3.393	0.9188	0.6626	4.049	−0.4119	0.5198	−3.666	−1.371
$N = 9$	−0.8215	−3.393	0.9188	0.6628	4.049	−0.4119	0.5198	−3.667	−1.371
[48]	–	–	0.9189	0.663	4.051	−0.412	0.520	−3.669	−1.37

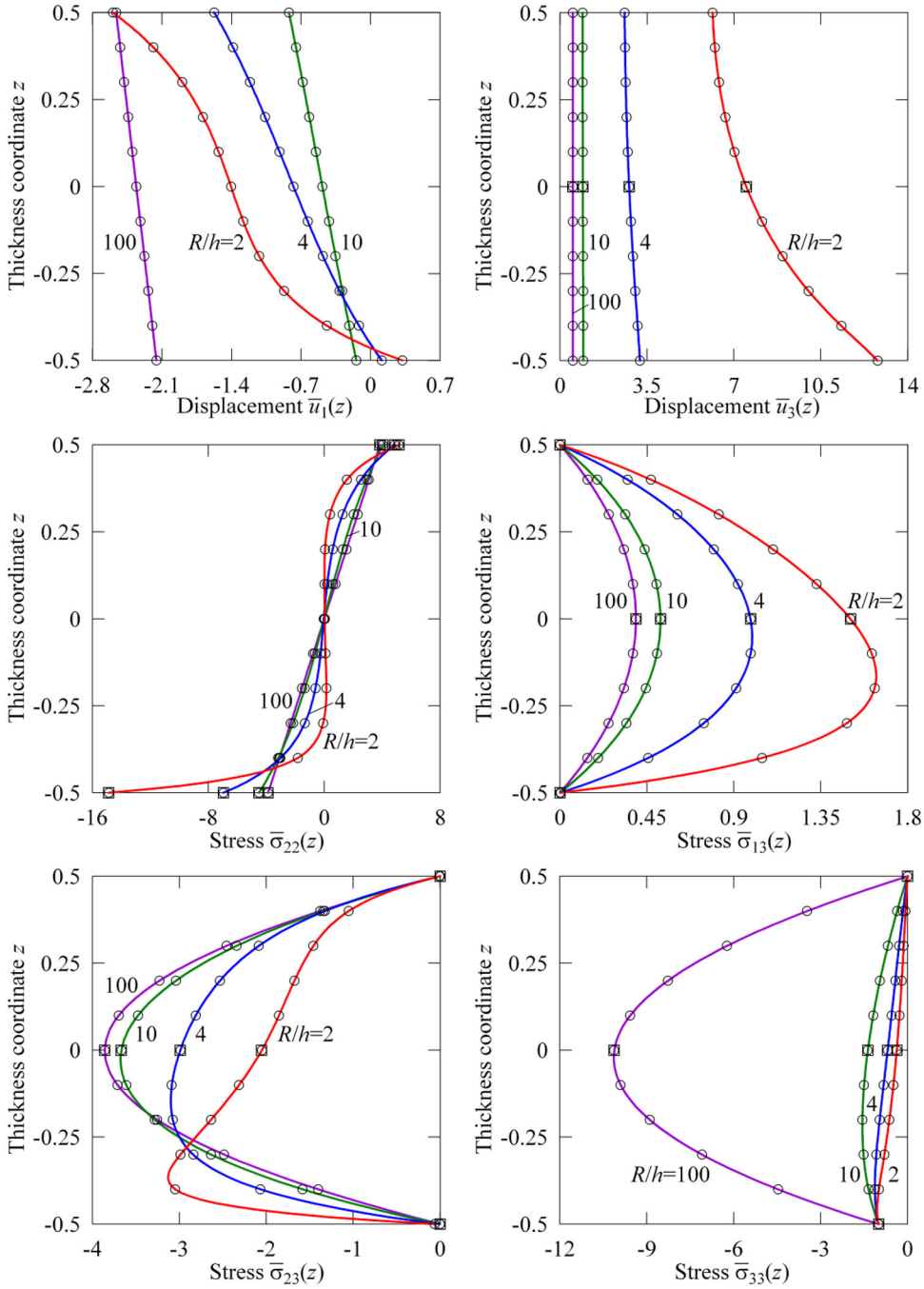

Figure 8. Through-thickness distributions of displacements and stresses for a composite cylindrical shell with $N = 9$ using 64×64 mesh; GeXSaS4 element (—), exact SaS solution [31] (○) and Varadan–Bhaskar exact solution [48] (□).

It is assumed that the Young modulus is distributed through the shell thickness according to the exponential law (44) with $E^- = 10^7$, whereas Poisson's ratio $\nu = 0.3$. The geometric parameters of the shell are $R = 1$ and $\theta_0 = \pi/18000$. To analyze the results efficiently, we introduce the dimensionless variables as functions of the dimensionless thickness coordinate as follows:

$$\begin{aligned} \bar{u}_3(z) &= 10Ehu_3(\pi/2, 0, z)/R^2p_0, \\ \bar{\sigma}_{11}(z) &= 10h\sigma_{11}(\pi/2, 0, z)/Rp_0, \\ \bar{\sigma}_{33}(z) &= \sigma_{33}(\pi/2, 0, z)/p_0, z = \theta_3/h, \end{aligned} \tag{48}$$

where

$$p_0 = 1.$$

Table 4 lists the results of the convergence study due to increasing the number of SaS for a very thick spherical shell using a fine 128×1 mesh. A comparison with the exact Lamé's solution for the homogeneous spherical shell [54] is also given. As it turned out, the GeXSaS4 element provides already four right digits for the displacement and stresses starting respectively from five and nine SaS. Figure 13 shows the through-thickness distributions of stresses for different values of the material gradient index α choosing seven SaS and 64×1 mesh. One can see that the boundary conditions on inner and outer surfaces for the transverse normal stress are satisfied again correctly with a high accuracy. The results of the convergence study due to mesh refinement through the normalized transverse displacement

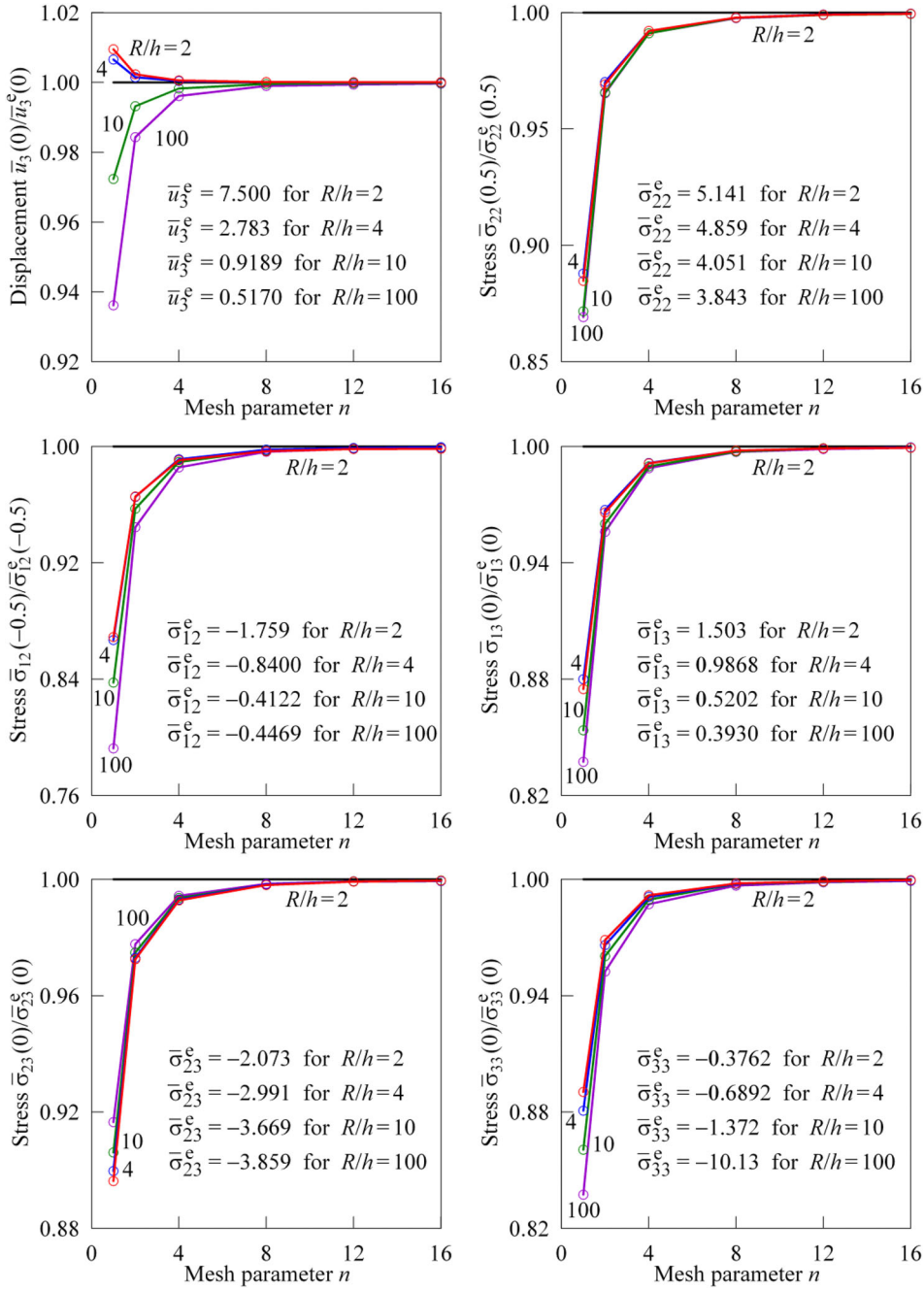

Figure 9. Convergence study due to mesh refinement for a composite cylindrical shell with $N = 9$ by using regular $4n \times 4n$ meshes with $n = 1, 2, 4, 8, 12$ and 16; reference values are provided by the exact SaS solution [31] choosing nine SaS.

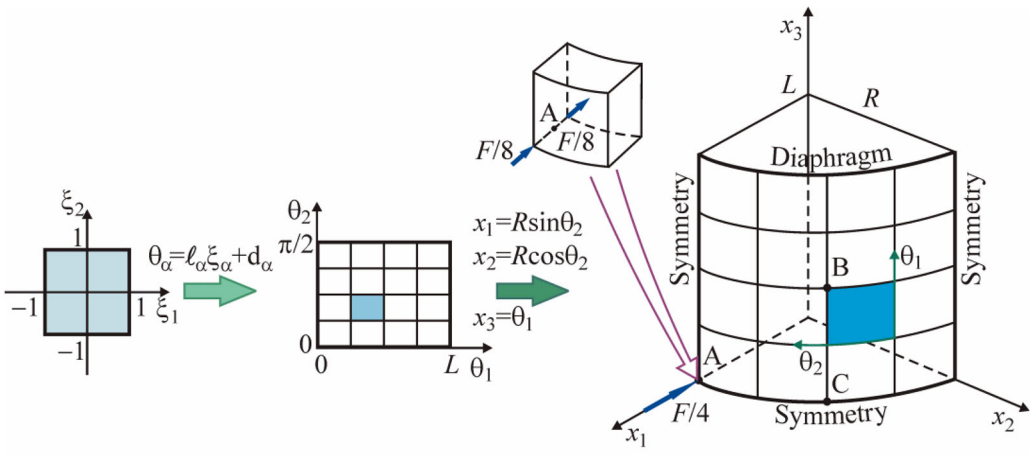

Figure 10. One octant of the pinched cylindrical shell modeled by regular $4n \times 4n$ meshes with $n = 1, 2, 4, 8, 16$ and 32.

Table 2. Convergence study for a pinched cylindrical shell with $R/h = 100$ using the transverse displacement $10^5 \times u_3(\mathrm{A}, 0)$.

Mesh	3 SaS	5 SaS	Solid45 [53] 2 elements	Solid45 [53] 4 elements	[50]	[51]	[52]
4×4	−1.555	−1.555	–	–	−0.681	−0.856	−0.728
8×8	−1.673	−1.674	−0.738	−0.738	−1.363	−1.443	−1.392
16×16	−1.779	−1.780	−1.520	−1.519	−1.706	−1.726	−1.706
32×32	−1.821	−1.823	−1.774	−1.774	–	–	–
64×64	−1.837	−1.839	−1.830	−1.831	–	–	–
128×128	−1.843	−1.845	−1.843	−1.844	–	–	–

Table 3. Convergence study for a pinched cylindrical shell with $R/h = 100$ using 64×64 mesh.

	$\bar{u}_1(\mathrm{B}, 0)$	$\bar{u}_3(\mathrm{B}, 0)$	$\bar{\sigma}_{11}(\mathrm{B}, 0.5)$	$\bar{\sigma}_{22}(\mathrm{B}, 0.5)$	$\bar{\sigma}_{12}(\mathrm{B}, 0.5)$	$\bar{\sigma}_{13}(\mathrm{B}, 0)$	$\bar{\sigma}_{23}(\mathrm{B}, 0)$	$\bar{\sigma}_{33}(\mathrm{C}, 0)$
$N = 3$	1.321	0.1362	2.545	−0.3242	−0.7405	0.5261	−3.920	0.0989
$N = 4$	1.321	0.1362	2.544	−0.3256	−0.7405	0.7335	−5.470	0.3924
$N = 5$	1.321	0.1362	2.544	−0.3254	−0.7405	0.7334	−5.475	0.3932
$N = 6$	1.321	0.1362	2.544	−0.3252	−0.7405	0.7333	−5.475	0.3928

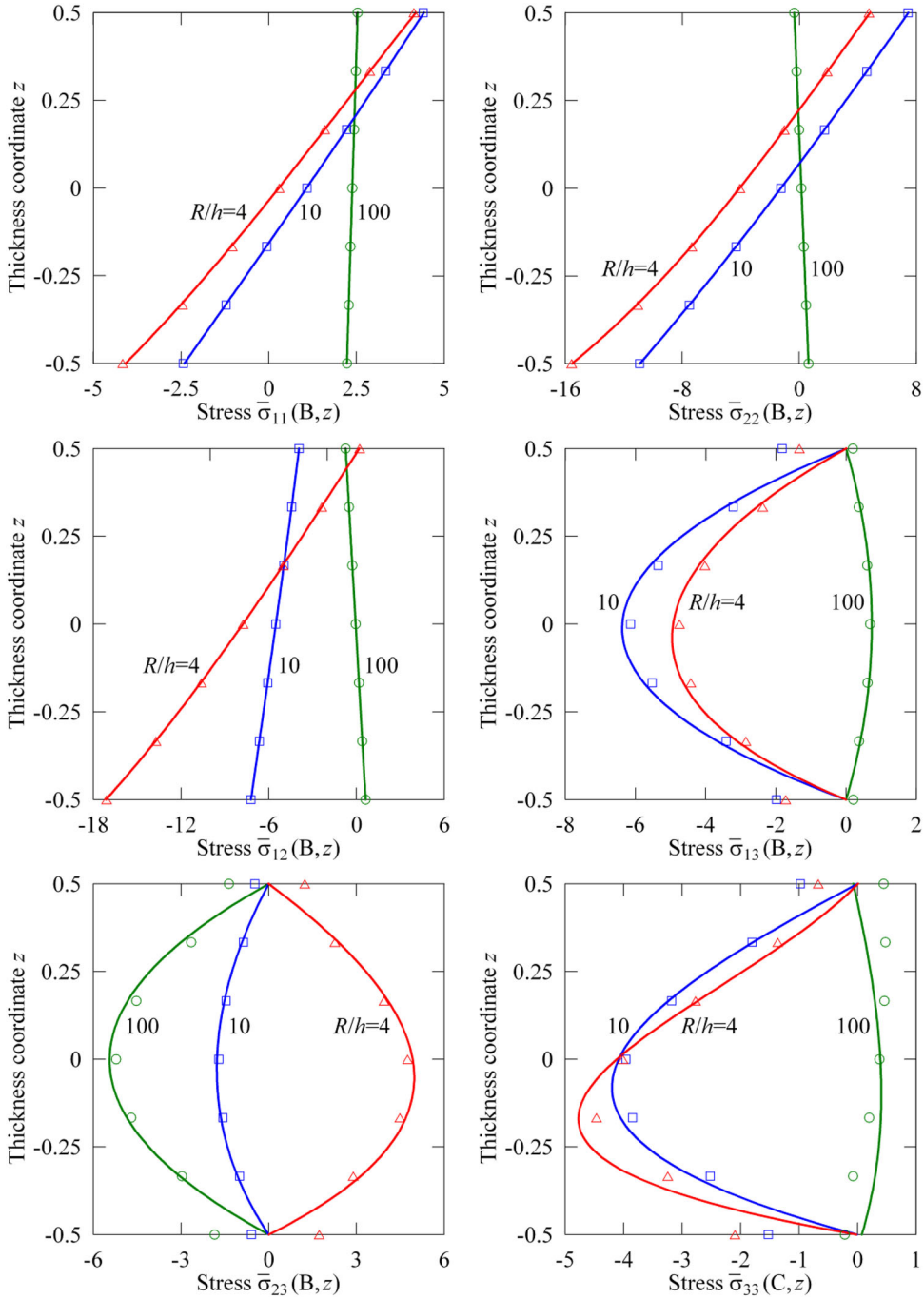

Figure 11. Through-thickness distributions of stresses for a pinched cylindrical shell with $N = 7$ using 64×64 mesh; GeXSaS4 element (—) and Solid45 element [53] with six elements in the thickness direction for $R/h = 4$ (Δ), $R/h = 10$ (□) and $R/h = 100$ (○).

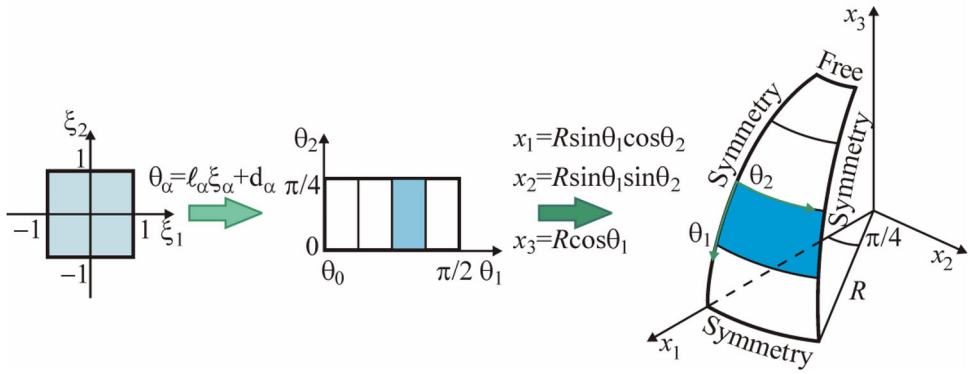

Figure 12. One sixteenth of the nonhomogeneous spherical shell modeled by regular $4n \times 1$ meshes with $n = 1, 2, 4, 8, 12, 16$ and 32.

Table 4. Convergence study for homogeneous and nonhomogeneous spherical shells with $R/h = 2$ using 128×1 mesh.

	$\alpha = 0$				$\alpha = 1$			
	$\bar{u}_3(0)$	$\bar{\sigma}_{11}(-0.5)$	$\bar{\sigma}_{11}(0.5)$	$\bar{\sigma}_{33}(0)$	$\bar{u}_3(0)$	$\bar{\sigma}_{11}(-0.5)$	$\bar{\sigma}_{11}(0.5)$	$\bar{\sigma}_{33}(0)$
$N = 3$	2.287	5.249	2.489	−0.3783	1.456	3.402	4.137	−0.5187
$N = 5$	2.300	4.609	2.090	−0.2575	1.449	2.470	3.557	−0.3363
$N = 7$	2.300	4.568	2.067	−0.2628	1.450	2.403	3.512	−0.3458
$N = 9$	2.300	4.566	2.066	−0.2626	1.450	2.400	3.510	−0.3455
[54]	2.300	4.566	2.066	−0.2626	–	–	–	–

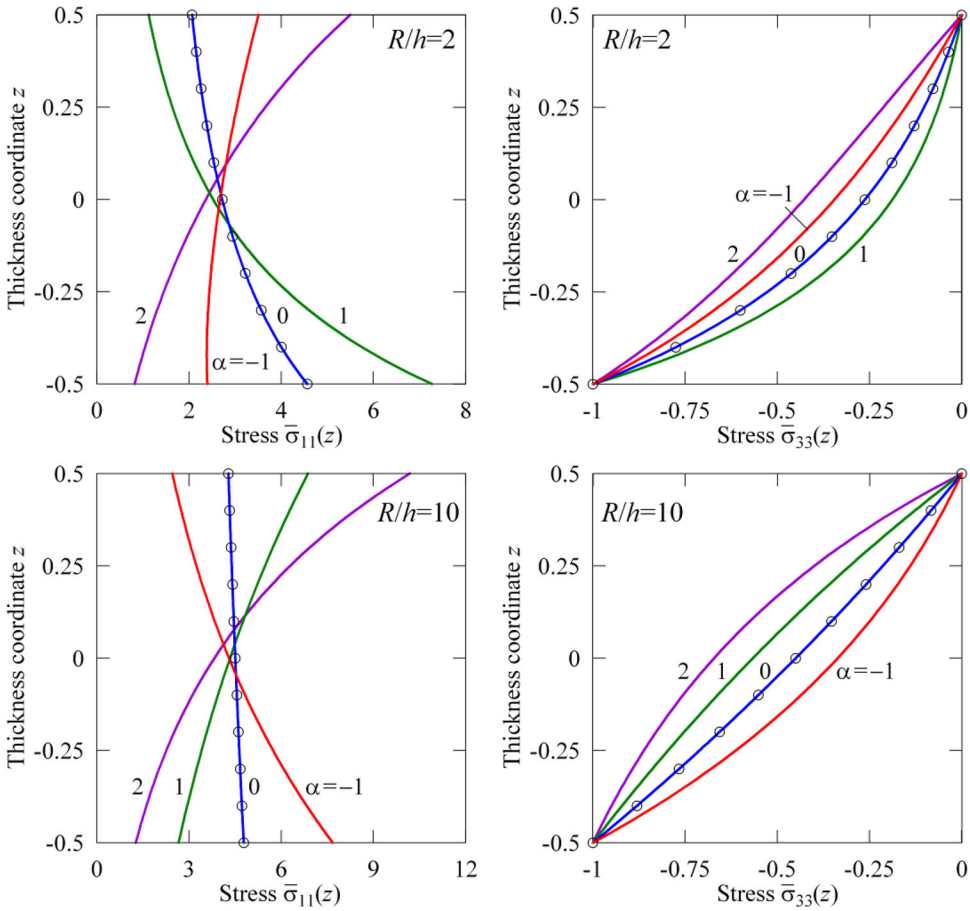

Figure 13. Through-thickness distributions of stresses for a spherical shell with $N = 7$ using 64×1 mesh; GeXSaS4 element (—) and Lamé's exact solution [54] (○).

and stresses for the same number of SaS are presented in Figure 14. The reference values are provided by Lamé's exact solution. As can be seen, the developed GeXSaS4 solid-shell element behaves well even for very thin shells in the case of coarse meshes except for the transverse normal stress.

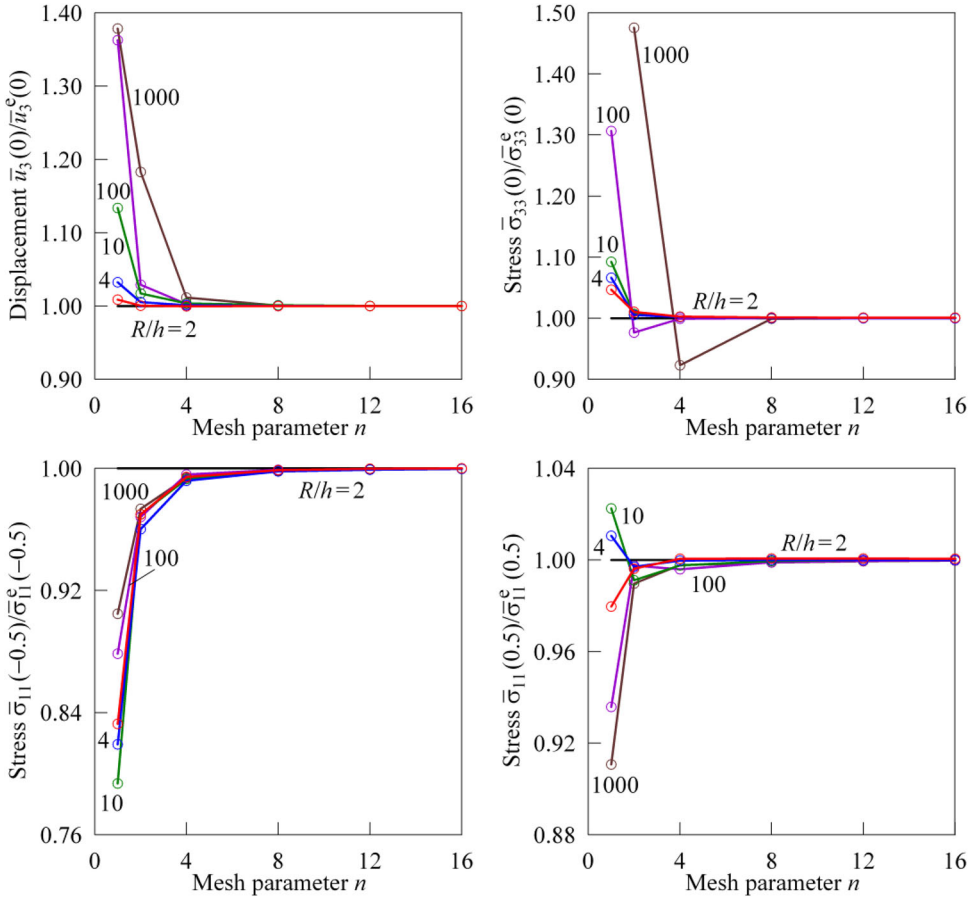

Figure 14. Convergence study due to mesh refinement for a homogeneous spherical shell under inner pressure with $N = 7$ by using regular $4n \times 1$ meshes with $n = 1, 2, 4, 8, 12$ and 16; reference values are provided by Lamé's exact solution [54].

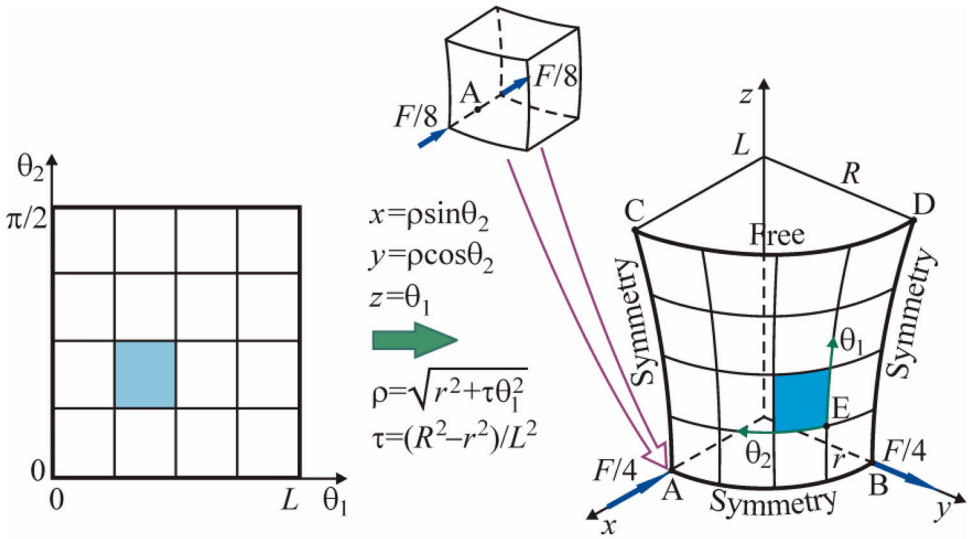

Figure 15. One octant of the pinched hyperbolic shell modeled by regular $4n \times 4n$ meshes with $n = 1, 2, 4, 8$ and 16.

8.4. Pinched FG hyperbolic shell

Finally, we study a FG hyperbolic shell under two pairs of opposite forces. The shell parameters are chosen to be $r = 7.5$, $R = 15$, $L = 20$, $h = 0.1$ and $F = 4$. This problem is a good benchmark to test the proposed analytical integration schemes because we deal here with a doubly-curved shell with variable coefficients of the first and second fundamental forms of the middle surface (parameters ρ and τ are given in Figure 15):

$$A_1 = \sqrt{1 + \frac{\tau^2\theta_1^2}{\rho^2}}, \quad A_2 = \rho, \quad k_1 = -\frac{\tau r^2}{\rho^3 A_1^3}, \quad k_2 = \frac{1}{\rho A_1},$$
$$B_1 = 0, B_2 = \frac{\tau\theta_1}{\rho^2 A_1}, \theta_1 \in [0, L]. \tag{49}$$

It is assumed that the shell is fabricated by mixing the metal and ceramic phases. For evaluating the effective material properties through the thickness of a two-phase shell, the Mori–Tanaka method [55, 56] is adopted

$$
\begin{aligned}
K &= K_{\mathrm{m}} + \frac{V_{\mathrm{c}}(K_{\mathrm{c}}-K_{\mathrm{m}})}{1+V_m(K_{\mathrm{c}}-K_{\mathrm{m}})/(K_{\mathrm{m}}+4G_m/3)},\\
G &= G_{\mathrm{m}} + \frac{V_{\mathrm{c}}(G_{\mathrm{c}}-G_{\mathrm{m}})}{1+V_m(G_{\mathrm{c}}-G_{\mathrm{m}})/(G_{\mathrm{m}}+f_{\mathrm{m}})},\\
f_{\mathrm{m}} &= \frac{G_{\mathrm{m}}(9K_{\mathrm{m}}+8G_{\mathrm{m}})}{6(K_{\mathrm{m}}+2G_{\mathrm{m}})},\\
K_{\mathrm{m}} &= \frac{E_{\mathrm{m}}}{3(1-2\nu_{\mathrm{m}})}, K_{\mathrm{c}} = \frac{E_{\mathrm{c}}}{3(1-2\nu_{\mathrm{c}})},\\
G_{\mathrm{m}} &= \frac{E_{\mathrm{m}}}{2(1+\nu_{\mathrm{m}})}, G_{\mathrm{c}} = \frac{E_{\mathrm{c}}}{2(1+\nu_{\mathrm{c}})},
\end{aligned}
\tag{50}
$$

where E_{m} and E_{c} are the Young moduli of metal and ceramic phases; ν_{m} and ν_{c} are the Poisson's ratios; G_{m} and G_{c} are the shear moduli; K_{m} and K_{c} are the bulk moduli; V_{m} and V_{c} are the volume fractions defined as

$$
V_{\mathrm{m}} = 1-V_{\mathrm{c}}, \quad V_{\mathrm{c}} = V_{\mathrm{c}}^{-} + \left(V_{\mathrm{c}}^{+}-V_{\mathrm{c}}^{-}\right)(0.5+z)^{\alpha}, \quad z = \theta_3/h,
\tag{51}
$$

where V_{c}^{-} and V_{c}^{+} are the volume fractions of the ceramic phase on the bottom and top surfaces; α is the material gradient index. The metal phase is taken to be aluminum with the material properties $E_{\mathrm{m}} = 7\times10^{10}$ Pa and $\nu_{\mathrm{m}} = 0.3$; the material properties of the ceramic are $E_{\mathrm{c}} = 4.27\times10^{11}$Pa and $\nu_{\mathrm{c}} = 0.17$. The calculations were performed for $V_{\mathrm{c}}^{-} = 0$ and $\alpha = 2$ choosing two values of the volume fraction of the ceramic phase on the top surface $V_{\mathrm{c}}^{+} = 0$ and 0.8. It is

Table 5. Convergence study for pinched homogeneous and FG hyperbolic shells using the displacement $\bar{u}_x = 10^6 \times u_x$ at points A and C.

Mesh	$V_{\mathrm{c}}^{+}=0$				$V_{\mathrm{c}}^{+}=0.8$					
	$N=3$		$N=5$		$N=3$		$N=5$		$N=7$	
	$-\bar{u}_x$(A)	$\bar{u}_x$(C)	$-\bar{u}_x$(A)	$\bar{u}_x$(C)	$-\bar{u}_x$(A)	$\bar{u}_x$(C)	$-\bar{u}_x$(A)	$\bar{u}_x$(C)	$-\bar{u}_x$(A)	$\bar{u}_x$(C)
4 × 4	1.555	1.776	1.555	1.776	0.983	1.124	0.967	1.106	0.968	1.107
8 × 8	1.683	1.703	1.683	1.703	1.063	1.077	1.046	1.060	1.047	1.060
16 × 16	1.720	1.684	1.721	1.684	1.087	1.065	1.069	1.048	1.070	1.048
32 × 32	1.731	1.680	1.731	1.680	1.093	1.062	1.076	1.045	1.077	1.046
64 × 64	1.734	1.679	1.734	1.679	1.095	1.061	1.078	1.044	1.079	1.045

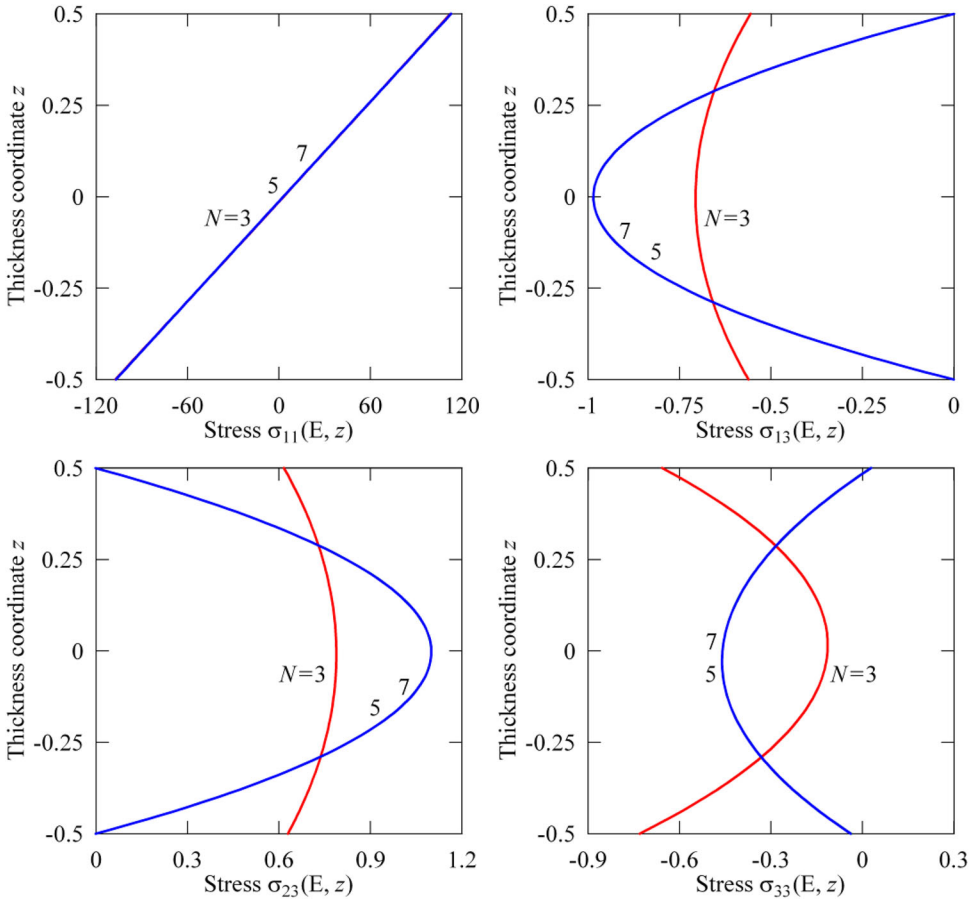

Figure 16. Through-thickness distributions of stresses for a pinched hyperbolic shell with $V_{\mathrm{c}}^{+} = 0$ using 64 × 64 mesh.

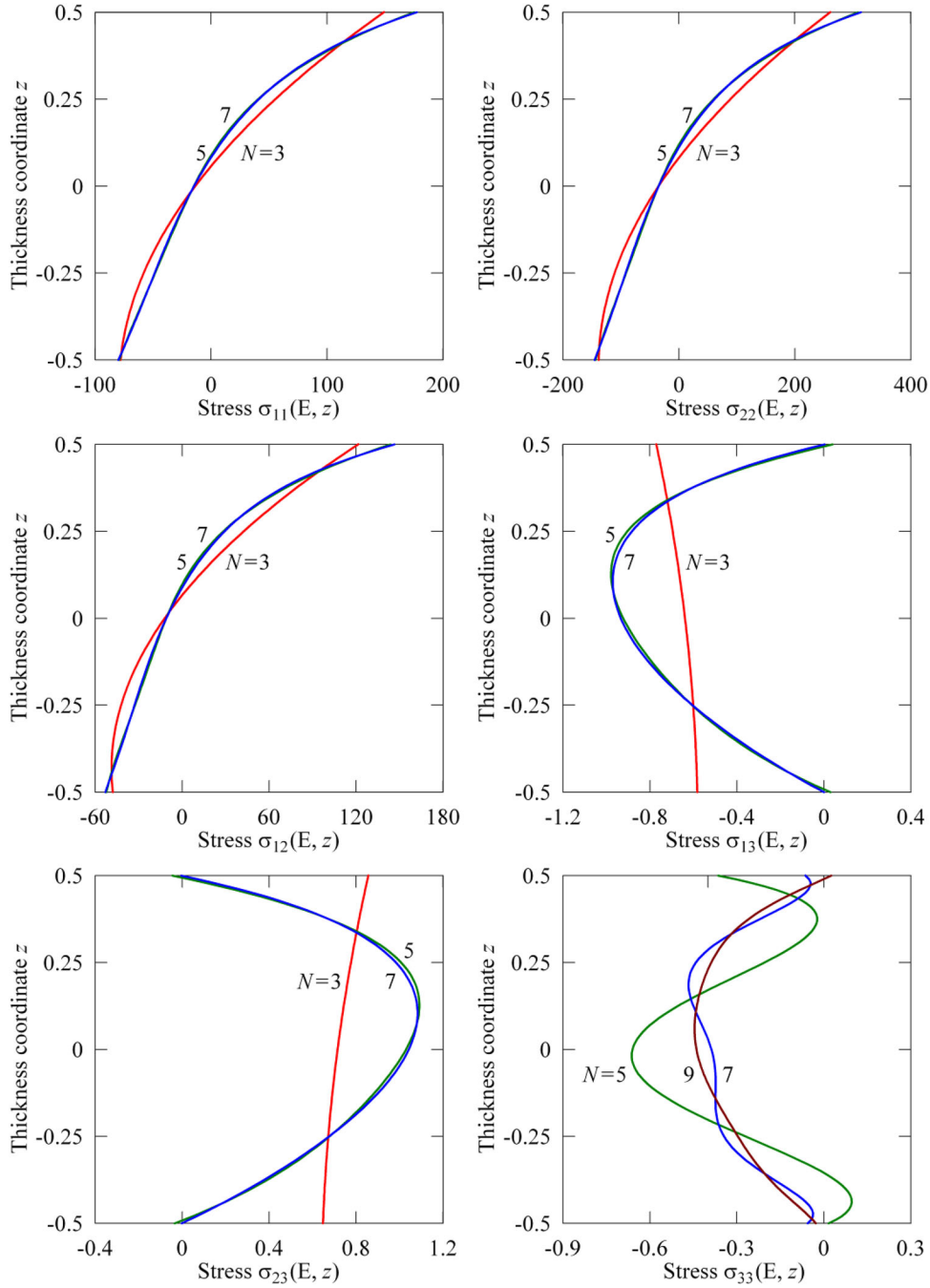

Figure 17. Through-thickness distributions of stresses for a pinched hyperbolic shell with $V_c^+ = 0.8$ using 64×64 mesh.

apparent that the first value corresponds to the homogeneous hyperbolic shell.

Due to symmetry of the problem, only one octant of the shell is discretized by regular meshes depicted in Figure 15. Table 5 shows the displacements of the middle surface at points A and C for a different number of SaS and meshes. Figures 16 and 17 present the through-thickness distributions of stresses at point $\mathrm{E}(L/4, \pi/8)$ belonging to the middle surface. As can be seen, the use of the 9-parameter shell model [24] based on the quadratic polynomial interpolation of displacements in the thickness direction that corresponds to the choice of three SaS yields a poor prediction for the transverse stresses. To satisfy the boundary conditions on bottom and top surfaces for these stress components with a high accuracy, we have to employ more SaS. Actually, five and seven SaS must be taken to describe correctly the transverse stress distributions in homogeneous and FG hyperbolic shells, respectively.

9. Conclusions

This paper presents the GeX hybrid-mixed ANS four-node solid-shell elements based on the SaS concept in which the displacements of SaS are utilized as fundamental shell unknowns. All SaS are located at Chebyshev polynomial nodes inside the shell that allows one to minimize uniformly the error caused by using the high order Lagrange interpolations for displacements, strains, stresses, and material

properties through the thickness. The element stiffness matrix of the FG shell is evaluated by means of 3D analytical integration with no expensive matrix inversion that is impossible with existing isoparametric hybrid-mixed solid-shell elements. The GeXSaS4 solid-shell element developed passes the zero energy mode test and 3D membrane and bending patch tests [47], and exhibits a superior performance in the case of coarse mesh configurations in all considered benchmarks. It can be recommended for the 3D stress analysis of thick and thin FG shell structures due to the fact that the SaS solutions asymptotically approach the 3D solutions of elasticity as the number of SaS tends to infinity.

Funding

This work was supported by the Russian Science Foundation (Grant No. 18-19-00092) and the Russian Ministry of Education and Science (Grant No. 9.4914.2017/6.7).

References

[1] J. J. Rhiu, and S. W. Lee, "A new efficient mixed formulation for thin shell finite element models," Int. J. Numer. Meth. Eng., vol. 24, no. 3, pp. 581–604, 1987.

[2] Y. H. Kim, and S. W. Lee, "A solid element formulation for large deflection analysis of composite shell structures," Comp. Struct., vol. 30, no. 1–2, pp. 269–274, 1988.

[3] N. Büchter, E. Ramm, and D. Roehl, "Three-dimensional extension of nonlinear shell formulation based on the enhanced assumed strain concept," Int. J. Numer. Meth. Eng., vol. 37, no. 15, pp. 2551–2568, 1994.

[4] K. Y. Sze, S. Yi, and M. H. Tay, "An explicit hybrid stabilized eighteen-node solid element for thin shell analysis," Int. J. Numer. Meth. Eng., vol. 40, no. 10, pp. 1839–1856, 1997.

[5] K. Y. Sze, W. K. Chan, and T. H. H. Pian, "An eight-node hybrid-stress solid-shell element for geometric non-linear analysis of elastic shells," Int. J. Numer. Meth. Eng., vol. 55, no. 7, pp. 853–878, 2002.

[6] G. M. Kulikov, and S. V. Plotnikova, "Non-linear strain-displacement equations exactly representing large rigid-body motions. Part I. Timoshenko-Mindlin Shell theory," Comput. Methods Appl. Mech. Eng., vol. 192, no. 7-8, pp. 851–875, 2003.

[7] G. M. Kulikov, and S. V. Plotnikova, "Non-linear geometrically exact assumed stress-strain four-node solid-shell element with high coarse-mesh accuracy," Finite Elem. Anal. Des., vol. 43, no. 6-7, pp. 425–443, 2007.

[8] S. Klinkel, F. Gruttmann, and W. Wagner, "A robust non-linear solid shell element based on a mixed variational formulation," Comput. Methods Appl. Mech. Eng, vol. 195, no. 1–3, pp. 179–201, 2006.

[9] H. Parisch, "A continuum-based shell theory for non-linear applications," Int. J. Numer. Meth. Eng., vol. 38, no. 11, pp. 1855–1883, 1995.

[10] Y. Başar, M. Itskov, and A. Eckstein, "Composite laminates: nonlinear interlaminar stress analysis by multi-layer shell elements," Comput. Methods Appl. Mech. Eng, vol. 185, no. 2–4, pp. 367–397, 2000.

[11] N. El-Abbasi, and S. A. Meguid, "A new shell element accounting for through-thickness deformation," Comput. Methods Appl. Mech. Eng., vol. 189, no. 3, pp. 841–862, 2000.

[12] N. El-Abbasi, and S. A. Meguid, "Finite element modeling of the thermoelastic behavior of functionally graded plates and shells," Int. J. Comp. Eng. Sci., vol. 01, no. 01, pp. 151–165, 2000.

[13] C. Sansour, and F. G. Kollmann, "Families of 4-node and 9-node finite elements for a finite deformation shell theory. An assessment of hybrid stress, hybrid strain and enhanced strain elements," Comput. Mech., vol. 24, no. 6, pp. 435–447, 2000.

[14] B. Brank, J. Korelc, and A. Ibrahimbegović, "Nonlinear shell problem formulation accounting for through-the-thickness stretching and its finite element implementation," Comput. Struct., vol. 80, no. 9–10, pp. 699–717, 2002.

[15] B. Brank, "Nonlinear shell models with seven kinematic parameters," Comput. Methods Appl. Mech. Eng., vol. 194, no. 21–24, pp. 2336–2362, 2005.

[16] R. A. Arciniega, and J. N. Reddy, "Tensor-based finite element formulation for geometrically nonlinear analysis of shell structures," Comput. Methods Appl. Mech. Eng., vol. 196, no. 4–6, pp. 1048–1073, 2007.

[17] R. A. Arciniega, and J. N. Reddy, "Large deformation analysis of functionally graded shells," Int. J. Solids Struct., vol. 44, no. 6, pp. 2036–2052, 2007.

[18] G. M. Kulikov, and S. V. Plotnikova, "Finite rotation geometrically exact four-node solid-shell element with seven displacement degrees of freedom," Comput. Model. Eng. Sci., vol. 28, pp. 15–38, 2008.

[19] K. Lee, and S. W. Lee, "An assumed strain solid shell element formulation with transversely quadratic displacement," Comput. Model. Eng. Sci., vol. 34, pp. 253–272, 2008.

[20] G. M. Kulikov, and S. V. Plotnikova, "Calculation of composite structures subjected to follower loads by using a geometrically exact shell element," Mech. Compos. Mater., vol. 45, no. 6, pp. 545–556, 2009.

[21] H. B. Coda, R. R. Paccola, and M. S. M. Sampaio, "Positional description applied to the solution of geometrically non-linear plates and shells," Finite Elem. Anal. Des., vol. 67, pp. 66–75, 2013.

[22] G. S. Payette, and J. N. Reddy, "A seven-parameter spectral/hp finite element formulation for isotropic, laminated composite and functionally graded shell structures," Comput. Methods Appl. Mech. Eng., vol. 278, pp. 664–704, 2014.

[23] H. B. Coda, R. R. Paccola, and R. Carrazedo, "Zig-Zag effect without degrees of freedom in linear and nonlinear analysis of laminated plates and shells," Compos. Struct., vol. 161, pp. 32–50, 2017.

[24] G. M. Kulikov, and S. V. Plotnikova, "Non-linear exact geometry 12-node solid-shell element with three translational degrees of freedom per node," Int. J. Numer. Meth. Eng., vol. 88, no. 13, pp. 1363–1389, 2011.

[25] G. M. Kulikov, and S. V. Plotnikova, "The use of 9-parameter shell theory for development of exact geometry 12-node quadrilateral piezoelectric laminated solid-shell elements," Mech. Adv. Mater. Struct., vol. 22, no. 6, pp. 490–502, 2015.

[26] M. Cinefra, E. Carrera, L. D. Croce, and C. Chinosi, "Refined shell elements for the analysis of functionally graded structures," Compos. Struct., vol. 94, no. 2, pp. 415–422, 2012.

[27] M. Cinefra, and E. Carrera, "Shell finite elements with different through-the-thickness kinematics for the linear analysis of cylindrical multilayered structures," Int. J. Numer. Meth. Eng., vol. 93, no. 2, pp. 160–182, 2013.

[28] E. Carrera, M. Cinefra, M. Petrolo, and E. Zappino, Finite Element Analysis of Structures through Unified Formulation, John Wiley & Sons, Chichester, West Sussex, 2014.

[29] T. H. C. Le, M. D'Ottavio, P. Vidal, and O. Polit, "A new robust quadrilateral four-node variable kinematics plate element for composite structures," Finite Elem. Anal. Des., vol. 133, pp. 10–24, 2017.

[30] P. Vidal, L. Gallimard, and O. Polit, "Robust layerwise C^0 finite element approach based on a variable separation method for the modeling of composite and sandwich plates," Finite Elem. Anal. Des., vol. 139, pp. 1–13, 2018.

[31] G. M. Kulikov, and S. V. Plotnikova, "On the use of sampling surfaces method for solution of 3D elasticity problems for thick shells," ZAMM - J. Appl. Math. Mech., vol. 92, no. 11–12, pp. 910–920, 2012.

[32] G. M. Kulikov, and S. V. Plotnikova, "On the use of a new concept of sampling surfaces in a shell theory," Adv. Struct. Mater., vol. 15, pp. 715–726, 2011.

[33] G. M. Kulikov, A. A. Mamontov, S. V. Plotnikova, and S. A. Mamontov, "Exact geometry solid-shell element based on a sampling surfaces technique for 3D stress analysis of doubly-curved composite shells," Curved Layered Struct., vol. 3, pp. 1–16, 2016.
[34] G. M. Kulikov, S. V. Plotnikova, and E. Carrera, "A robust, four-node, quadrilateral element for stress analysis of functionally graded plates through higher-order theories," Mech. Adv. Mater. Struct., vol. 25, pp. 1, 2017. doi: 10.1080/15376494.2017.1288994.
[35] N. S. Bakhvalov, Numerical Methods: Analysis, Algebra, Ordinary Differential Equations, MIR Publishers, Moscow, 1977.
[36] T. H. H. Pian, "State-of-the-art development of hybrid/mixed finite element method," Finite Elem. Anal. Des., vol. 21, no. 1–2, pp. 5–20, 1995.
[37] T. H. H. Pian, and K. Sumihara, "Rational approach for assumed stress finite elements," Int. J. Numer. Meth. Eng., vol. 20, no. 9, pp. 1685–1695, 1984.
[38] S. W. Lee, and T. H. H. Pian, "Improvement of plate and shell finite elements by mixed formulations," Aiaa J, vol. 16, no. 1, pp. 29–34, 1978.
[39] G. Wempner, D. Talaslidis, and C. M. Hwang, "A simple and efficient approximation of shells via finite quadrilateral elements," J. Appl. Mech., vol. 49, no. 1, pp. 115–120, 1982.
[40] G. M. Kulikov, and S. V. Plotnikova, "Geometrically exact assumed stress-strain multilayered solid-shell elements based on the 3D analytical integration," Comput. Struct., vol. 84, no. 19–20, pp. 1275–1287, 2006.
[41] S. A. Ambartsumyan, Theory of Anisotropic Shells, NASA TT F-118, Washington, D.C., 1964.
[42] G. M. Kulikov, and S. V. Plotnikova, "Solution of three-dimensional problems for thick elastic shells by the method of reference surfaces," Mech. Solids., vol. 49, no. 4, pp. 403–412, 2014.
[43] T. J. R. Hughes, and T. E. Tezduyar, "Finite elements based upon mindlin plate theory with particular reference to the four-node bilinear isoparametric element," J. Appl. Mech., vol. 48, no. 3, pp. 587–596, 1981.
[44] K. J. Bathe, and E. N. Dvorkin, "A formulation of general shell elements - the use of mixed interpolation of tensorial components," Int. J. Numer. Meth. Eng., vol. 22, no. 3, pp. 697–722, 1986.
[45] Y. Ko, P. S. Lee, and K. J. Bathe, "A new MITC4+ shell element," Comput. Struct, vol. 182, pp. 404–418, 2017.
[46] P. Betsch, and E. Stein, "An assumed strain approach avoiding artificial thickness straining for a nonlinear 4-node shell element," Commun. Numer. Meth. Engng., vol. 11, no. 11, pp. 899–909, 1995.
[47] G. M. Kulikov, and S. V. Plotnikova, "A hybrid-mixed four-node quadrilateral plate element based on sampling surfaces method for 3D stress analysis," Int. J. Numer. Meth. Eng., vol. 108, no. 1, pp. 26–54, 2016.
[48] T. K. Varadan, and K. Bhaskar, "Bending of laminated orthotropic cylindrical shells - an elasticity approach," Compos. Struct., vol. 17, no. 2, pp. 141–156, 1991.
[49] T. Belytschko, B. L. Wong, and H. Stolarski, "Assumed strain stabilization procedure for the 9-node lagrange shell element," Int. J. Numer. Meth. Eng., vol. 28, no. 2, pp. 385–414, 1989.
[50] T. J. R. Hughes, and W. K. Liu, "Nonlinear finite element analysis of shells. Part II: two-dimensional shells," Comput. Methods Appl. Mech. Eng., vol. 27, no. 2, pp. 167–181, 1981.
[51] W. K. Liu, E. S. Law, D. Lam, and T. Belytschko, "Resultant-stress degenerated-shell element," Comput. Methods Appl. Mech. Eng., vol. 55, no. 3, pp. 259–300, 1986.
[52] J. C. Simo, D. D. Fox, and M. S. Rifai, "On a stress resultant geometrically exact shell model. Part II: the linear theory; computational aspects," Comput. Methods Appl. Mech. Eng., vol. 73, no. 1, pp. 53–92, 1989.
[53] ANSYS Release 5.6, ANSYS Inc, Canonsburg, PA, 1999.
[54] S. P. Timoshenko, and J. N. Goodier, Theory of Elasticity, McGraw-Hill, New York, 1970.
[55] T. Mori, and K. Tanaka, "Average stress in matrix and average elastic energy of materials with misfitting inclusions," Acta Metall., vol. 21, no. 5, pp. 571–574, 1973.
[56] Y. Benveniste, "A new approach to the application of Mori–Tanaka's theory in composite materials," Mech. Mater., vol. 6, pp. 147–157, 1987.

Appendix A

According to Eqs. (7), (10), (23), (24), and (27) the nodal strain parameters of SaS can be written as

$$\lambda^I_{i\alpha r} = \left(\Xi^I_{i\alpha r}\right)^{\mathrm{T}}\mathbf{q},\ \beta^I_{ir} = \left(\Xi^I_{i3r}\right)^{\mathrm{T}}\mathbf{q}, \tag{A1}$$

where Ξ^I_{ijr} are the *constant* inside the element vectors of order $12N$ given by

$$\begin{gathered}
\left(\Xi^I_{i\alpha r}\right)_{i+3(I-1)+3N(s-1)} = d_{\alpha rs},\ \ \left(\Xi^I_{i3r}\right)_{i+3(J-1)+3N(s-1)} = \delta_{rs}M^J\left(\theta^I_3\right),\\
\left(\Xi^I_{\alpha\alpha r}\right)_{\beta+3(I-1)+3N(s-1)} = \delta_{rs}B_{\alpha s},\ \ \left(\Xi^I_{\alpha\beta r}\right)_{\beta+3(I-1)+3N(s-1)} = -\delta_{rs}B_{\beta s}\ \text{for}\ \beta\neq\alpha,\\
\left(\Xi^I_{\alpha\alpha r}\right)_{3+3(I-1)+3N(s-1)} = \delta_{rs}k_{\alpha s},\ \ \left(\Xi^I_{3\alpha r}\right)_{\alpha+3(I-1)+3N(s-1)} = -\delta_{rs}k_{\alpha s},\\
d_{\alpha rs} = \frac{1}{4\ell_\alpha A_{\alpha r}}n_{\alpha s}\left(1+n_{\beta r}n_{\beta s}\right)\ \text{for}\ \beta\neq\alpha,
\end{gathered} \tag{A2}$$

where $A_{\alpha r}$, $k_{\alpha r}$, and $B_{\alpha r}$ are the nodal values of the geometric parameters of the middle surface; δ_{rs} is the Kronecker delta. The parameters $n_{\alpha r}$ are defined by Eq. (24) and, as we remember, the indices $i,j=1,2,3$; $\alpha,\beta=1,2$; $r,s=1,2,3,4$; $I,J=1,2,\ldots,N$. The remaining components of vectors not written out are zero.

Using Eqs. (6), (25), (26), and (A1), we arrive at the explicit form of the strain-displacement matrices introduced in Section 5:

$$\mathbf{B}^I_r = \begin{bmatrix}
\left(c^I_{1r}\right)^{-1}\left(\Xi^I_{11r}\right)^{\mathrm{T}}\\
\left(c^I_{2r}\right)^{-1}\left(\Xi^I_{22r}\right)^{\mathrm{T}}\\
\left(\Xi^I_{33r}\right)^{\mathrm{T}}\\
\left(c^I_{2r}\right)^{-1}\left(\Xi^I_{12r}\right)^{\mathrm{T}} + \left(c^I_{1r}\right)^{-1}\left(\Xi^I_{21r}\right)^{\mathrm{T}}\\
\left(c^I_{1r}\right)^{-1}\left(\Xi^I_{31r}\right)^{\mathrm{T}} + \left(\Xi^I_{13r}\right)^{\mathrm{T}}\\
\left(c^I_{2r}\right)^{-1}\left(\Xi^I_{32r}\right)^{\mathrm{T}} + \left(\Xi^I_{23r}\right)^{\mathrm{T}}
\end{bmatrix}, \tag{A3}$$

where $c^I_{\alpha r} = 1 + k_{\alpha r}\theta^I_3$ are the nodal values of the shifter tensor on SaS.

Appendix B

Here, we study the matrix of weighted coefficients from Eq. (20).

Proposition B1. The determinant of the matrix $\mathbf{\Gamma} = [\Gamma^{IJ}]$ is not equal to zero.

Proof. Introduce any vector $\mathbf{v} = [v_1 v_2 \ldots v_N]^{\mathrm{T}}$ and consider a quadratic form

$$\mathbf{v}^{\mathrm{T}}\mathbf{\Gamma}\mathbf{v} = \sum_I\sum_J \Gamma^{IJ}v_Iv_J = \sum_I\sum_J v_Iv_J\int_{-h/2}^{h/2} L^IL^Jc_1c_2d\theta_3 = \int_{-h/2}^{h/2} g^2c_1c_2d\theta_3, \tag{B1}$$

where

$$g(\theta_3) = \sum_I L^Iv_I. \tag{B2}$$

Because of $c_\alpha > 0$ the quadratic form $\mathbf{v}^{\mathrm{T}}\mathbf{\Gamma}\mathbf{v}$ is positive definite and, therefore, $\det\mathbf{\Gamma} > 0$ □.